Loss of Bcl6 transcriptionally alters classical dendritic cells and diminishes T follicular helper cell and Th17-inducing cDC2 in mice

Hongkui Xiao[1,*], Isabel Ulmert[1,*], Johanna Huber[2], Hamsa Narasimhan[3,4], Luisa Bach[5], Ilia Kurochkin[6,7], Urs Mörbe[1], Lili Zhang[8], Andreas Schlitzer[8], Filipe Pereira[6,7,9], Barbara U. Schraml[3,4], Dirk Baumjohann[2,4], Katharina Lahl[1,10]

Affiliations:

[1]Section for Experimental and Translational Immunology, Institute for Health Technology, Technical University of Denmark (DTU), 2800 Kongens Lyngby, Denmark

[2]Institute for Immunology, Biomedical Center, Faculty of Medicine, LMU Munich, Planegg-Martinsried, Germany.

[3]Biomedical Center, Institute of Cardiovascular Physiology and Pathophysiology, Faculty of Medicine, Ludwig-Maximillians-Universität München, Planegg-Martinsried, Germany.

[4]Walter-Brendel-Centre of Experimental Medicine, University Hospital, LMU Munich, Planegg-Martinsried, Germany

[5]Medical Clinic III for Oncology, Hematology, Immuno-Oncology and Rheumatology, University Hospital Bonn, University of Bonn, Bonn, Germany.

[6]Cell Reprogramming in Hematopoiesis and Immunity Laboratory, Lund Stem Cell Center, Molecular Medicine and Gene Therapy, Lund University, Lund, Sweden.

[7]Wallenberg Center for Molecular Medicine, Lund University, Lund, Sweden.

[8]Quantitative Systems Biology, Life and Medical Sciences (LIMES) Institute, University of Bonn, Germany.

[9]Center for Neuroscience and Cell Biology, University of Coimbra, Coimbra, Portugal.

[10]Immunology Section, Lund University, Lund 221 84, Sweden

*these authors contributed equally to this work

Corresponding authors: Katharina Lahl (1atharina.lahl@med.lu.se) and Dirk Baumjohann (dirk.baumjohann@uni-bonn.de)

Keywords: dendritic cells, transcriptional regulation, Bcl6, cDC1, cDC2, Tfh

ABSTRACT

Conventional dendritic cells (cDC) play key roles in immune induction, but what drives their heterogeneity and functional specialization is still ill-defined. Here we show that deletion of the transcriptional repressor Bcl6 in murine cDC alters the phenotype and transcriptome of cDC1 and cDC2, while their lineage identity is preserved. Bcl6-deficient cDC1 were diminished in the periphery but maintained their ability to cross-present antigen to $CD8^+$ T cells, confirming general maintenance of this subset. Surprisingly, the absence of Bcl6 in cDC caused a complete loss of Notch2-dependent cDC2 in the spleen and intestinal lamina propria. DC-targeted Bcl6-deficient mice induced fewer T follicular helper cells in response to the model antigen ovalbumin and mounted diminished Th17 immunity to *Citrobacter rodentium* in the colon. Our findings establish Bcl6 as an essential transcription factor for subsets of cDC and add to our understanding of the transcriptional landscape underlying cDC heterogeneity.

INTRODUCTION

Conventional dendritic cells (cDC) have the unique ability to present antigen to naïve T cells within lymphoid organs[1–3]. Upon encounter of antigen, migratory cDC scanning the peripheral environment mature and relocate to the draining lymph nodes (LNs), where they collaborate with LN-resident cDC to initiate immunity[4]. The spleen is the secondary lymphoid organ responsible for induction of immune responses to blood-derived antigen[5] and maturation of splenic cDC leads to similar relocation from the marginal zone and red pulp into the white pulp, where naïve B and T cells reside[6,7]. “Resident” resting DC are also found in the spleen, where they are located in the T cell zones in the absence of stimulation[8].

Conventional DC are broadly divided into two main subsets, cDC1 and cDC2[1]. cDC1 are characterized by their expression of the cDC1-exclusive chemokine receptor XCR1 and the absence of CD11b and Sirpα. Their development and functions are dependent on the transcription factors (TFs) IRF8[9,10], BATF3[11], Nfil3[12,13] and Id2[14] and they excel at cross-presenting antigen to $CD8^+$ T cells, which is at least in part attributable to their ability to engulf apoptotic

57 material[15–19]. cDC2 express high levels of CD11b and Sirpα, but not XCR1, and the transcriptional
58 network governing their development is less well defined. cDC2 show a higher level of
59 heterogeneity than cDC1[20] and recent attempts to subset cDC2 further have suggested
60 separation based on Notch2 versus Klf4-dependency[21]. IRF4-deficiency leads to a partial loss of
61 cDC2 and is thought to impact primarily on their survival and ability to migrate[22–24]. Other TFs
62 reported to influence cDC2 development or function include ZEB2[25], IRF-2[26] and Rel-B[27]. In the
63 spleen, the majority of cDC2 express endothelial cell specific adhesion marker (ESAM), a marker
64 defining cDC2 located in the bridging channels of the marginal zone, where they fulfill critical
65 functions in activating $CD4^+$ T cells and germinal center (GC) formation[28,29]. The development of
66 $ESAM^{hi}$ cDC2 depends on Notch2-signaling induced by delta ligand 1 (DLL1) expressed by stromal
67 cells[22,28,30,31] and on the chemokine receptor Ebi2 (GPR183)[32].

68 The TF Bcl6 plays an essential role in GC reactions, being required for the differentiation of both
69 GC B cells and T follicular helper (Tfh) cells in a cell intrinsic manner[33]. Bcl6 is expressed in cDC1,
70 and to a lower extent in cDC2[20] and we have shown previously that complete Bcl6-deficiency
71 causes a loss of $CD11b^-$ DC, presumed to be cDC1[20]. Other work has confirmed that Bcl6-deficient
72 mice lack splenic CD8-expressing cDC1, but also reported a reduction in splenic $CD4^+$ cDC2[34].
73 However, a more recent study has disputed these findings, by showing normal cDC1 numbers in
74 mice with conditional *Bcl6* deletion driven by cre recombinase under the control of the *Csf1*
75 promoter. Importantly, these authors suggested that down-regulation of CD11c in the absence
76 of Bcl6 may have compromised the detection of cDC1 in the earlier studies[35].

77 Here we reconcile these conflicting data by performing in-depth analysis of the cDC compartment
78 in mice lacking Bcl6 in all cDC or specifically in cDC1, using CD11c- and Clec9a- or XCR1-driven cre
79 drivers, respectively. Our results show that while cDC1 showed substantial alterations in gene
80 expression including deregulation of genes involved in cytokine signaling and cell adhesion, their
81 ability to cross-present antigen was largely conserved in the absence of Bcl6. Bcl6-deficiency in
82 DC led to a complete loss of the Notch2-dependent $ESAM^{hi}$ cDC2 subset in the spleen and
83 consequently to a defect in splenic Tfh cell induction to ovalbumin as a model antigen. Likewise,
84 Notch2-dependent cDC2 in the intestinal lamina propria (LP) were reduced in the absence of Bcl6
85 in DC, leading to a decrease in Th17-responses and delayed healing upon infection with the

86 enteric pathogen *Citrobacter rodentium*. Our findings suggest that the core subset identities of
87 cDC1 and cDC2 are maintained in the absence of Bcl6, but that its deficiency in DC causes cell-
88 intrinsic, subset-specific alterations in DC abundance and function, which translates into
89 corresponding defects in adaptive immune responses.

90

91 **RESULTS**

92 **Bcl6 deficiency alters DC subset phenotypes and numbers across tissues**

93 We have previously shown that mice completely lacking Bcl6 are largely devoid of CD11b^{-} cDC,
94 presumed to be cDC1[20]. To better define the impact of Bcl6-deficiency on cDC1, we generated
95 mice lacking Bcl6 specifically in cDC1 by crossing XCR1.cre mice to mice carrying a floxed Bcl6
96 gene (*XCR1.Bcl6^{KO}*). Additionally, we deleted Bcl6 in all CD11c-expressing cells by crossing
97 CD11c.cre mice to Bcl6^{flox} mice (*CD11c.Bcl6^{KO}*). As controls, we used the respective cre negative
98 Bcl6^{flox} littermates (designated as control throughout). As expected, flow cytometry revealed
99 mutually exclusive populations of CD11c^{+}MHCII^{+} cDC in control spleens based on the expression
100 of XCR1 or CD11b to identify cDC1 and cDC2, respectively. However, there was a clear population
101 of XCR1^{+}CD11b^{+} cDC in the absence of Bcl6 in the spleens of both Bcl6-deficient mouse lines (Fig.
102 1A). XCR1^{+}CD11b^{+} cDC were also abundant within the resident populations of peripheral and
103 mesenteric lymph node (pLN and mLN) cDC in the absence of Bcl6 (Fig. 1B). The absolute numbers
104 of total XCR1^{+} cDC (independent of CD11b expression) were only mildly reduced in *XCR1.Bcl6^{KO}*
105 and normal in *CD11c.Bcl6^{KO}* mice, while XCR1^{-}CD11b^{+} cDC were significantly diminished in
106 *CD11c.Bcl6^{KO}* mice, but normal in *XCR1.Bcl6^{KO}* mice (Fig. 1A). Resident cDC numbers were not
107 substantially altered in either pLNs or mLNs (Fig. 1B).

108 We next analyzed migratory DC populations in different organs. Mice lacking Bcl6 in cDC1 or in
109 all DC had significantly fewer migratory XCR1^{+} cDC in pLNs and mLNs and these also expressed
110 CD11b (Fig. 2A). Interestingly, we also detected a loss of XCR1^{-}CD103^{+}CD11b^{+} cDC in the
111 migratory compartment of the mLNs of *CD11c.Bcl6^{KO}* mice, whereas the numbers of XCR1^{-}CD103^{-}
112 CD11b^{+} cDC were normal (Fig. 2A). As the majority of migratory cDC in the mLNs derives from the
113 small intestinal lamina propria (SILP), we next analyzed this compartment. There were fewer

114 XCR1^{+} cDC in the SILP of both *XCR1.Bcl6^{KO}* and *CD11c.Bcl6^{KO}* mice, all of which again expressed
115 CD11b (Fig. 2B). In addition, the numbers of XCR1^{-}CD103^{+}CD11b^{+} cDC were reduced in
116 *CD11c.Bcl6^{KO}* mice, while the numbers of XCR1^{-}CD103^{-}CD11b^{+} cDC were less affected (Fig. 2B).
117 Together these results suggest that the decreases in migratory XCR1^{+} and XCR1^{-}CD103^{+}CD11b^{+}
118 cDC seen in mLNs are caused by absence of these populations, rather than a disability to migrate.
119 Similar changes in cDC were seen in the lung in the absence of Bcl6, with reduced numbers and
120 upregulation of CD11b in XCR1^{+} cDC in both *XCR1.Bcl6^{KO}* and *CD11c.Bcl6^{KO}* mice, together with
121 reduced numbers of XCR1^{-}CD11b^{+} cDC in *CD11c.Bcl6^{KO}* mice (Suppl. Fig. 1A). Thus, Bcl6 deficiency
122 affects cDC in several locations.

123

124 **cDC1 and cDC2 signatures are preserved in the absence of Bcl6 in DC**

125 One of the most surprising findings from our studies was the expression of the cDC2 marker
126 CD11b by the XCR1^{+} cDC that was preserved in Bcl6-deficient mice. To determine whether this
127 reflects acquisition of CD11b by cDC1, or cDC2 with aberrant XCR1 expression, we sorted splenic
128 XCR1^{+} cDC (independent of CD11b expression) and XCR1^{-}CD11b^{+} cDC from control, *XCR1.Bcl6^{KO}*
129 and *CD11c.Bcl6^{KO}* mice for bulk mRNA-sequencing (see Fig. 1A for gating). Principal component
130 (PC) analysis showed that XCR1^{+} cDC segregated from XCR1^{-}CD11b^{+} cDC in all mouse models
131 along PC axis 1, which accounted for 69% of the variance. This strongly supports the idea that
132 Bcl6-deficient cDC1 and cDC2 maintained overall lineage identity (Fig. 3A). Nevertheless, PC2
133 separated the populations on the basis of Bcl6 presence or absence, accounting for 13% of the
134 variance and suggesting that Bcl6 has a significant impact on the gene transcription profile of
135 both cDC1 and cDC2. Interestingly, cDC1 from *XCR1.Bcl6^{KO}* and *CD11c.Bcl6^{KO}* mice clustered
136 closely and were separated from control cDC1, while cDC2 in *CD11c.Bcl6^{KO}* mice segregated from
137 those in *XCR1.Bcl6^{KO}* and control mice, consistent with XCR1-cre being specific to cDC1 and
138 indicating that Bcl6 regulates gene expression in both cDC subsets in a cell-intrinsic manner. PC3
139 accounted for 4% of the variance and showed opposite directional bias in Bcl6-deficient cDC1
140 and cDC2 (Fig. 3A). This suggests that Bcl6-mediated regulation of gene transcription may affect
141 some targets in cDC1 and cDC2 differently.

142 To explore further how Bcl6 might regulate cDC lineage identity, we generated cDC1 and cDC2
143 signatures by identifying the top 50 genes that were differentially expressed between our control
144 cDC1 and cDC2 and interrogated how these signatures were affected by a loss of Bcl6 expression
145 (for gene lists and expression levels see Suppl. Table 1). Supporting their maintenance of lineage
146 identity, XCR1$^+$ cDC from both *XCR1.Bcl6^{KO}* and *CD11c.Bcl6^{KO}* mice retained the expression of
147 cDC1 markers, including *Irf8*, *Tlr3*, *Clec9a*, and *Cadm1* (Fig. 3B). However, *Cd8a* was
148 downregulated in Bcl6-deficient XCR1$^+$ cDC and several genes associated with cDC2 identity were
149 upregulated by XCR1$^+$ cDC in the absence of Bcl6, including *Sirpa*, *Zeb2*, *Csf1r* and *Itgam* (encoding
150 CD11b) (foldchange > 2, padjust < 0.01). Although Bcl6-deficient CD11b$^+$ cDC2 did not express
151 cDC1 specific markers, cDC2 from *CD11c.Bcl6^{KO}* mice showed altered expression of several
152 classical cDC2 markers, of which some were further upregulated such as *Csf1*, *Zeb2* and *Itgam*,
153 while others were downregulated, including *Clec4a4* and *CD4* (Fig. 3B). Despite maintenance of
154 core lineage expression patterns, the overall transcriptional profiles of XCR1$^+$ and XCR1$^-$CD11b$^+$
155 cDC were significantly altered in the absence of Bcl6 (Fig. 3A, C). In total, 607 genes were
156 differentially regulated in XCR1$^+$ cDC from *XCR1.Bcl6^{KO}* mice compared with control cDC1, with
157 473 being upregulated and 134 downregulated. In contrast, of the 452 differentially regulated
158 genes in cDC2 from *CD11c.Bcl6^{KO}* mice, only 206 were upregulated, compared with 246
159 downregulated genes (Fig. 3D, for list of contributing genes see Suppl. Table 2). Interestingly, only
160 79 genes were coordinately overexpressed in Bcl6-deficient cDC1 and cDC2, and 32 genes were
161 coordinately downregulated in the absence of Bcl6 in both subsets. 12 genes were reciprocally
162 regulated in the two subsets, of which 11 genes were upregulated in cDC1 and downregulated in
163 cDC2 (including receptor encoding genes *Ffar1* and *Lair1,* enzyme-encoding genes *Tgm2, Pigv*
164 and *Malt1* and genes encoding proteins implicated in cellular and intracellular adhesion and
165 transport *Cdh17, Ctnnd2, Ston2 and Rin2*). The gene for the actin-binding protein Plectin was the
166 only gene upregulated in cDC2 and downregulated in cDC1. Taken together, although the lineage
167 identity of splenic cDC1 and cDC2 is generally maintained in the absence of Bcl6, this does result
168 in significant changes in subset-specific gene expression in both cDC subsets.

169

170 **Bcl6-deficiency in cDC1 causes alterations in immunologically relevant pathways**

171 To better characterize the impact of Bcl6-deficiency on cDC1, we next compared the expression
172 of cDC1-related markers using flow cytometry. This confirmed the maintenance of Tlr3, Xcr1, Irf8,
173 CD103 and Clec9a expression by XCR1$^+$ cDC from the spleen of *XCR1.Bcl6^{KO}* mice, as well as
174 upregulation of CD11b and Sirpα and loss of CD8α (Fig. 4A). In addition, we detected higher
175 expression of the costimulatory ligand CD24 on Bcl6-deficient cDC1. Next, we analyzed how the
176 absence of Bcl6 might influence the immunological functions of cDC1 by performing gene set
177 enrichment analysis of the RNA-Seq data from XCR1$^+$ cDC in *XCR1.Bcl6^{KO}* and control mice. This
178 showed that several immunologically relevant gene ontology pathways were enriched within the
179 differentially expressed gene sets, including *leukocyte adhesion*, *proliferation* and *activation*, as
180 well as *production of IL-1* (Fig. 4B). In parallel, KEGG pathway analysis highlighted differences in
181 *cytokine-cytokine receptor interactions, NOD-like receptor signaling pathway, MERK signaling*
182 *pathway, hematopoiesis cell lineage, Tuberculosis* and *C-type lectin receptor signaling pathway*
183 (Fig. 4C, D). These data suggest that Bcl6-mediated transcriptional repression in cDC1 may tune
184 the function of this subset.

185

186 **Bcl6-deficient cDC1 maintain the ability to cross-present antigen**

187 The most characteristic property of cDC1 is to cross-present exogenous antigen to class I MHC-
188 restricted CD8$^+$ T cells, a function which involves cell-surface receptors such as Clec9A (Dngr1)
189 that mediate the uptake of dead cells[18,19]. Our gene expression analysis suggested that XCR1$^+$
190 cDC1 maintained the expression of *Clec9a* in the absence of Bcl6 and this was confirmed by flow
191 cytometry (Fig. 4A). We therefore examined whether cross-presentation was intact in
192 *XCR1.Bcl6^{KO}* animals by injecting heat-killed ovalbumin-expressing mouse embryonic fibroblasts
193 (OVA-MEFs) into recipient mice adoptively transferred with OVA-specific TCR-transgenic CD8$^+$ T
194 cells from OT-I mice. OT-I proliferation strictly depends on cDC1-mediated cross-presentation in
195 this model[17]. OT-I cells proliferated to a similar extent in the spleens of OVA-MEF injected
196 *XCR1.Bcl6^{KO}* and control mice (Fig. 5A, B), suggesting that Bcl6-deficient cDC1 retain their ability
197 to cross-present. OTI proliferation was also observed in the mLN. In the mLN of *XCR1.Bcl6^{KO}* mice
198 OTI cells showed somewhat diminished proliferation compared to control mice, however, this

199 most likely reflects the decreased number of migratory cDC1 in the mLN of *XCR1.Bcl6^{KO}* mice (Fig.
200 2A).

201 Taken together, although cDC1-specific Bcl6 deficiency alters the phenotype and transcriptional
202 profile of cDC1, the hallmark function of cDC1 to cross-present antigen is largely unaffected by
203 the loss of Bcl6.

204

205 **Bcl6-deficiency results in a selective loss of Notch2-dependent cDC2**

206 In addition to its role in cDC1, our initial results also revealed a significant role for Bcl6 in the gene
207 expression signature of cDC2. Furthermore, the numbers of cDC2 were reduced in the spleen of
208 *CD11c.Bcl6^{KO}* mice, as were the numbers of cDC2 expressing CD103 in the intestinal LP and mLNs.
209 Diminished cDC2 numbers in the blood of CD11c.Bcl6^{KO} mice suggest that this was not due to a
210 release of cDC2 into the bloodstream (Suppl. Fig. 1B). The remaining cDC in the spleen of
211 *CD11c.Bcl6^{KO}* mice also showed somewhat lower expression of MHCII and higher expression of
212 CD11b than control cDC2 (Fig. 6A). Further phenotyping of spleen cDC2 in *CD11c.Bcl6^{KO}* mice
213 revealed a striking loss of the ESAM^{hi} cDC2 subset (Fig 6B and Suppl. Fig. 2). We verified our
214 findings an independent mouse model in which Bcl6 deletion was induced by cre recombinase
215 under the control of the *Clec9a* promoter, which targets cDC precursors and their progeny and
216 some pDCs but no other leukocytes[36]. These mice additionally carry a YFP reporter following a
217 floxed stop cassette in the ubiquitous ROSA26 locus to monitor targeting efficiency. As in
218 *CD11c.Bcl6^{KO}* mice, spleen cDC in *Clec9a.Bcl6^{KO}* mice showed altered CD11b expression and loss
219 of ESAM^{hi} cDC2 (Fig. 6C, D and Suppl. Fig. 2). This was apparent in the analysis of bulk cDC2 in
220 *Clec9a.Bcl6^{KO}* mice and was even more pronounced when examining the YFP^{+} cDC2, which are
221 enriched for cDC2 with a history of *Clec9a*-promoter activity (Fig. 6E).

222 As expected[28], the ESAM^{lo} subset of cDC2 expressed slightly lower levels of CD11c compared to
223 their ESAM^{hi} counterparts and a significant proportion lacked expression of 33D1 and CD4, which
224 were expressed uniformly by ESAM^{hi} cDC2 (Fig. 6F). The total population of cDC2 remaining in
225 *CD11c.Bcl6^{KO}* mice resembled the ESAM^{lo} population in terms of these markers but expressed

226 higher levels of CD11b and IRF4 than either ESAM^{hi} or ESAM^{lo} control cDC2 subset, suggesting
227 these markers may be specific targets of Bcl6 repression.

228 To explore the nature of the cDC2 remaining in the spleen of *CD11c.Bcl6^{KO}* mice further, we
229 performed gene set enrichment analysis (GSEA) of differentially expressed genes between
230 *CD11c.Bcl6^{KO}* and control cDC2 in gene sets derived from publicly available bulk RNA-Seq data
231 from ESAM^{hi} and ESAM^{lo} cDC2 from control spleen[37]. As expected from their usual predominance
232 in control spleen, control cDC2 gene signatures were highly enriched in ESAM^{hi} vs ESAM^{lo} gene
233 sets, while *CD11c.Bcl6^{KO}* cDC2 gene signatures were highly enriched in ESAM^{lo} vs ESAM^{hi} gene
234 sets (Fig. 7A). We next directly compared the set of genes that was differentially expressed in
235 ESAM^{hi} vs ESAM^{lo} cDC2 with the gene set differentially expressed in *CD11c.Bcl6^{KO}* vs control cDC2.
236 In accordance with the GSEA data, the majority of the top 50 genes expressed more prominently
237 by ESAM^{hi} cDC2 were also significantly over-represented in the population of total control cDC2,
238 which expressed much fewer of the top 50 genes from ESAM^{lo} cDC2 (Fig. 7B). Conversely, the
239 genes over-expressed by total cDC2 from *CD11c.Bcl6^{KO}* spleen showed much more overlap with
240 the top 50 genes expressed by ESAM^{lo} cDC2, while the genes over-expressed by ESAM^{hi} cDC2
241 were mostly downregulated in Bcl6-deficient cDC2 (Fig. 7B, for a complete gene list containing
242 expression levels see Suppl. Table 3). These data confirm that Bcl6 deficiency in DC causes the
243 loss of the ESAM^{hi} lineage of splenic cDC2.

244

245 **DC-specific loss of Bcl6 causes defects in T follicular helper cell priming in the spleen**

246 ESAM^{hi} spleen DC reside in the marginal zone bridging channels, where they play a prominent
247 role in the induction of germinal centers[29]. Confocal microscopy using CD11c as a pan-DC marker
248 and TLR3 and Sirpα to define cDC1 and cDC2, respectively, confirmed a substantial loss of DC
249 from this region in the *CD11c.Bcl6^{KO}* spleen (Fig. 7C). To test the functional relevance of this
250 defect, we adoptively transferred OVA-specific TCR-transgenic CD4^{+} T cells (OT-II) into control
251 and *CD11c.Bcl6^{KO}* mice, immunized the mice with OVA + poly(I:C) intraperitoneally and assessed
252 the generation of antigen-specific Tfh cells three days later (Fig. 7D). We chose this timepoint
253 because this early Tfh cell induction is independent of GC B cells[38,39], which are known to express

254 CD11c and are required for the maintenance of Tfh cells at later times[40]. Although OT-II cells
255 expanded normally in the *CD11c.Bcl6*^{KO} mice in response to immunization, the early induction of
256 antigen-specific Tfh cells was markedly reduced in immunized *CD11c.Bcl6*^{KO} mice compared to
257 control mice (Fig. 7E), suggesting that Bcl6-dependent cDC indeed drive early Tfh cell induction
258 in this model. To enable analysis of later timepoints of the GC reaction and to confirm findings in
259 mice in which Bcl6 deletion is confined to cDC, we adoptively transferred naïve OT-II cells into
260 control or *Clec9a.Bcl6*^{KO} mice, followed by i.p. immunization with OVA in alum adjuvants and
261 analysis of the spleen seven days later (Fig. 7D,F). The frequency of CXCR5^{+}PD-1^{+} Tfh cells was
262 significantly reduced in OT-II cells recovered from *Clec9a.Bcl6*^{KO} hosts as compared to control
263 animals (Fig. 7F) and this was also the case for the endogenous Tfh cell pool in these mice. Thus,
264 Bcl6 deficiency in cDC causes the loss of ESAM^{hi} cDC2 and significantly impairs Tfh responses in
265 the spleen.

266

267 **DC-specific loss of Bcl6 causes defects in Th17 cell priming in the colon of mice infected with *C.***
268 ***rodentium***

269 In addition to their role in driving GC reactions in the spleen, Notch2-dependent cDC2 have been
270 shown to support Th17-dependent immunity towards *C. rodentium* in the colon[22]. The colonic LP
271 (cLP) of *CD11c.Bcl6*^{KO} mice contained significantly fewer cDC than that of control mice, with the
272 most pronounced loss detected in the CD103^{+} cDC2 population (Fig. 8A, B). To analyze whether
273 Bcl6-deficiency recapitulated the functional consequences of Notch2-deficiency, we infected
274 *CD11c.Bcl6*^{KO} and control littermates with *C. rodentium. CD11c.Bcl6*^{KO} mice lost comparable
275 weight to control littermates early after infection, with delayed recovery as evidenced by
276 significantly lower body weight from day 11 onwards (Fig. 8C). Consistent with a lack in weight
277 difference between genotypes at day nine post infection, colon length and bacterial load were
278 comparable at this time point, while there was a tendency towards shorter colons and elevated
279 bacterial load in *CD11c.Bcl6*^{KO} mice compared to control littermates 21 days post infection (Fig.
280 8C). At this late stage during infection, colons from *CD11c.Bcl6*^{KO} mice continued to show mild
281 pathology, while control littermates appeared fully healed (Fig. 8D). In parallel, there were

282 blunted Th17 responses in the cLP of *CD11c.Bcl6*^{KO} mice 9 days after *C. rodentium* infection (Fig.
283 8E), while Th1 and Treg numbers were not affected. This defect in Th17 priming was no longer
284 evident 21 days after infection (Fig. 8F).

285 These data show that Bcl6-deficiency in DC causes the loss of a prominent colonic cDC2 subset,
286 with a consequent defect in Th17 priming in response to *C. rodentium* infection, leading to
287 delayed healing and recovery.

288

289 **DISCUSSION**

290 We show here that Bcl6-deficiency in the DC compartment causes major transcriptional
291 alterations with subset-specific consequences. Specifically, Bcl6-deficient cDC1 acquire a
292 XCR1/CD11b double-positive phenotype not seen in control mice, where XCR1 and CD11b are
293 mutually exclusive markers of cDC1 and cDC2, respectively. However, Bcl6-deficient cDC1
294 retained a cDC1-like transcriptome, cDC1 lineage markers and the ability to cross-present. The
295 lack of Bcl6 in DC also revealed a critical role for Bcl6 in the development of the ESAM^{hi} subset of
296 cDC2 in the spleen and cDC2 in the intestines and there was a parallel defect in splenic Tfh cell
297 induction in response to protein antigen immunization and in intestinal Th17 induction in
298 response to *C. rodentium* infection. Together these findings extend the role of Bcl6 to the
299 regulation of cDC2 behavior in GC function and the periphery.

300 We previously described a selective loss of putative cDC1 in the spleen of Bcl6-deficient mice
301 based on the absence of CD8α^+CD11b$^-$ cDC[20]. Here we refine this interpretation by showing that
302 the numbers of resident cDC1 are in fact normal when Bcl6 is lacking in CD11c$^+$ cells or cDC1, but
303 they upregulate CD11b and down-regulate CD8α, causing them to merge into the classical cDC2
304 gate. In contrast, the numbers of migratory CD103$^+$CD11b$^-$ cDC1 are decreased in the mLN and
305 intestinal mucosa of mice lacking Bcl6 within the DC compartment, a finding supported by
306 defective cross presentation activity in the mLNs. We currently cannot explain the differential
307 effects of Bcl6 deficiency on resident versus migratory cDC1 populations. However, a similar
308 dichotomy has been described recently for dependence on DC-SCRIPT, whose absence

309 predominantly diminished resident cDC1[41]. As Bcl6 primarily acts as a transcriptional repressor,
310 it is possible that DC-SCRIPT and Bcl6 integrate in a feedback loop to regulate cDC1 migration or
311 survival upon maturation and this idea requires further study.

312 As Bcl6 is not expressed by DC progenitors in the bone marrow and their frequency is not affected
313 by the lack of Bcl6[35,42], Bcl6 seems to act downstream of other cDC1 lineage specifying TFs such
314 as IRF8, Nfil3, BATF3, DC-SCRIPT, and Id2. In models deficient of those TFs, the cDC1 lineage is
315 affected from the precursor level onwards, preventing their expression of all lineage markers, as
316 well as their ability to cross-present antigen[10,12–14,41,43–46], hallmarks that were preserved in Bcl6-
317 deficient cDC1. Rather, it appears that Bcl6 may fine-tune cDC1 identity by suppressing selected
318 cDC2 genes at the mature state and as a result, Bcl6-deficient cDC1 maintain key cDC1 genes such
319 as XCR1, TLR3, and CLEC9A as well as cross-presentation function. However, they show a gene
320 expression profile that suggests a cDC2-related "gain-of-function", with enhanced expression of
321 genes of the cytokine-cytokine receptor pathway, cell adhesion and migration pathways and
322 pathways associated with inflammasome activity. Interestingly, cDC1 with upregulated CD11b
323 and Sirpα have also been described when the TF ZEB2 is over-expressed from the pre-cDC stage
324 onwards[25]. Exploring how Bcl6 interacts with this and other lineage determining factors to
325 regulate cDC1 gene expression and functions will be an important topic for future research.

326 *CD11c.Bcl6^{KO}* and *Clec9a.Bcl6^{KO}* mice lacked the dominant subset of ESAM^{hi} cDC2 in the spleen
327 and comparison of gene expression profiles between ESAM^{hi} and ESAM^{lo} control cDC2 subsets
328 and cDC2 from *CD11c.Bcl6^{KO}* mice showed that Bcl6-deficient cDC2 closely aligned with control
329 ESAM^{lo} cDC2. However, this overlap was not absolute, suggesting that Bcl6-deficiency causes
330 transcriptional changes in all cDC2. For example, the extent of dysregulation of IRF4 and CD11b
331 expression in the absence of Bcl6 cannot solely be explained by the loss of ESAM^{hi} cDC2. In
332 addition, both markers were also upregulated in Bcl6-deficient cDC1, again indicating a wider
333 role for Bcl6 in control of mature cDC differentiation. Interestingly, the consequences of Bcl6
334 deficiency on cDC overlap with those previously shown for Notch2 deficiency[20,28,34]. Specifically,
335 both mice show deficiencies in cDC1 and ESAM^{hi} cDC2, but it remains to be determined whether
336 the apparent loss of cDC1 in Notch2-deficient animals reflects genuine absence of these cells, or
337 is because their phenotype has simply changed, as we show in Bcl6-deficient mice. Of note, the

338 cDC1 marker CD24 is upregulated in both Bcl6- and Notch2-targeted mice (our study and [22,28]),
339 arguing against a developmental defect within the cDC1 spleen compartment in Notch2-targeting
340 models. It will be of interest to explore how the Notch2- and Bcl6-pathways interact in DC biology.

341 Consistent with the findings that cDC2 equivalent to the ESAM^{hi} population locate preferentially
342 in marginal zone bridging channels in the spleen[47], the dysregulation in splenic cDC populations
343 in both Bcl6- and Notch2-deficient mice was associated with loss of cDC from this region of the
344 spleen ([29] and current results). Localization of cDC2 to the bridging channels is dependent on the
345 homing receptor GPR183[48,49] and Bcl6 regulates GPR183 expression in B cells[50]. However,
346 GPR183 expression levels were not altered in Bcl6-deficient cDC2, suggesting either that
347 additional factors are required for the correct positioning of cDC2 in the spleen, or that Bcl6-
348 deficiency causes a development block or diminished survival within ESAM^{hi} cDC2 irrespective of
349 their location. Along those lines, GPR183 deficiency in cDC2 specifically diminished antibody
350 response generation to particulate antigen, while responses to soluble antigen were
351 unaffected[49]. The defect in ESAM^{hi} cDC2 we found in *CD11c.Bcl6^{KO}* and *Clec9a.Bcl6^{KO}* mice was
352 accompanied by reduced induction of Tfh cells in response to parenteral immunization with
353 soluble OVA, suggesting a general deficiency in supporting GC reactions in these mice. While it
354 has been suggested that Notch2 is needed to ensure correct positioning of cDC2 for access to
355 antigen in the bloodstream[28], it has to our knowledge not been addressed whether response
356 deficits were limited to particulate antigen in these mice. Further investigation is needed to
357 explore the importance of correct localization on development, survival, and antigen capture by
358 cDC2 and how this might be controlled by a Bcl6-Notch2 axis.

359 XCR1^{-}CD103^{+}CD11b^{+} intestinal LP DC were also reduced in the absence of Bcl6 in DC, again
360 mirroring the phenotype observed in Notch2-deficient mice[22,28]. cDC2 are potent drivers of Th17
361 responses in the intestines[23,51], but recent findings suggest that DC-independent Th17 cell
362 induction can also occur[52]. As *CD11c.Notch2^{KO}* mice succumb early to *C. rodentium* infection due
363 to deficient IL-23 driven innate immunity, the adaptive immune response has not been
364 investigated in this model[22]. In contrast, the early stages of infection were normal in *CD11c.Bcl6^{KO}*
365 mice, but these mice showed a delay in recovery at later stages and altered kinetics of Th17
366 induction, with significantly lower Th17 numbers at day nine, which had normalized by day 21.

367 We cannot currently explain the differences in the early innate immune response between
368 *CD11c.Notch2*^{KO} and *CD11c.Bcl6*^{KO} mice, but our data are consistent with the idea that DC play
369 the dominant role in coordinating the adaptive immunity required to terminate infection.
370 However, while Bcl6-dependent cDC2 support optimal Th17 induction to *C. rodentium*, they are
371 not essential for this response, as Th17 numbers normalized over time.

372 Our results show that Bcl6 deficiency does not alter cDC1 and cDC2 lineage identity, but it alters
373 their transcriptional profile and relative abundance of both lineages and their subsets in different
374 tissues. Specifically, although cDC1 in all tissues examined acquired several cDC2 markers in the
375 absence of Bcl6, they retained their transcriptional and functional identity as cDC1. In contrast,
376 Bcl6 deficiency had differing effects on cDC2 subsets that depended on their location and
377 phenotype, with selective depletion of ESAM^{hi} cDC2 in spleen and CD103^{+}CD11b^{+} cDC2 in the
378 intestine. These effects were similar to those described for a deficiency in Notch2 and had
379 significant functional consequences for adaptive immunity in the spleen and intestine. These data
380 add to the emerging and poorly understood heterogeneity within the cDC2 compartment by
381 establishing that certain cDC2 subsets require Bcl6 in addition to Notch2- and lymphotoxin β-
382 signaling for their development. Finally, complementary to its established roles in controlling B
383 and T cell-intrinsic cell fate decisions[53], our findings establish Bcl6 as a subset-specific regulator
384 of DC development and function with critical consequences for the induction of adaptive immune
385 responses.

386

387 **MATERIALS AND METHODS**

388

389 **Mice**

390

391 *Xcr1.cre* (*B6-Xcr1*^{tm2Ciphe})[54], *CD11c.cre*[31] and *Clec9A.cre*[36] mice were crossed to *Bcl6*$^{fl/fl}$ mice[55]
392 (from Alexander Dent or JAX.org stock number #023727) to obtain DC-specific Bcl6-knockout
393 models. *Clec9A.Bcl6*^{KO} mice and *Clec9A.Bcl6*^{CONTROL} control mice were both maintained
394 homozygous for cre and additionally contained homozygous a *Rosa26*$^{fl\text{-}Stop\text{-}fl\text{-}YFP}$ allele (JAX.org
395 stock number 006148). *CD11c.Bcl6* and *XCR1.Bcl6* models were maintained heterozygous for cre

396 and negative littermates were used as control controls. Additional strains used in this study were
397 B6.SJL-Ptprc[a] Pepc[b]/BoyJ (congenic C57BL/6.CD45.1 mice from the Jackson Laboratory), C57BL/6-
398 Tg (Tcra Tcrb)1100Mjb/J and B6.Cg-Tg(TcraTcrb)425Cbn/J (OT-I and OT-II mice from Jackson
399 Laboratory). In some experiments, OT-II (Thy1.1) mice were used as donors. Mice were group-
400 housed in individually ventilated cages and maintained under specific pathogen-free conditions.
401 Experimental groups were sex and age-matched. Male and female littermates were used
402 between 8 and 15 weeks of age, RNA-Seq was performed on female mice only. All animal
403 experiments were performed in accordance with European regulation and federal law of
404 Denmark and Germany, either approved by the Danish Animal Experiments Inspectorate, the
405 Regierung von Oberbayern or the Landesamt für Natur-, Umwelt und Verbraucherschutz NRW.
406
407 **Cell preparation**
408
409 Spleens, mLNs and pLN (axillary, brachial and inguinal) were digested in RPMI containing 5% FCS,
410 0.5 mg/ml Collagenase IV and 15 µg/ml DNase I for 45 min at room temperature. Red blood cells
411 in spleen and blood samples were subsequently lysed using red blood cell lysis buffer (ammonium
412 chloride, potassium bicarbonate, EDTA, and MiliQ water) for 3 minutes at room temperature. For
413 the OT-II Thy1.1 adoptive transfer experiments, splenic single cell suspensions were prepared
414 and analyzed as previously described[56].
415
416 Single cell suspensions of the intestinal LP were prepared as described previously[57]. Briefly, the
417 intestines were flushed with HBSS supplemented with FCS (10 %), Peyer's patches were removed
418 and epithelial cells and mucus were removed by incubating tissue in HBSS supplemented with
419 FCS (10%) and EDTA (2 mM) 3 times each for 15 min at 37 °C with continual shaking at 450 rpm.
420 Remaining tissue pieces were digested in R10 media (RPMI 1640 supplemented with FCS (10 %)
421 containing DNase I grade II (30 µg/ml) and Liberase TM (58 µg/ml, Roche) for 20 min at 37 °C with
422 a magnetic stirrer.
423

424 Lungs were perfused with PBS prior to resection. All lung lobes were cut into small pieces and
425 digested in R5 media (RPMI 1640 supplemented with FCS (5 %) containing DNase I grade II (30
426 µg/ml) and Liberase TM (50 µg/ml, Roche) for 45 min at 37 °C with a magnetic stirrer.
427
428 Intestinal LP and lung cell suspensions were filtered through 100 µm cell strainers (Fisher
429 Scientific) and leukocytes were enriched by density gradient centrifugation with 40 % / 70 %
430 Percoll (GE Healthcare) prior to further analysis.
431
432 **Flow cytometry**
433
434 Single-cell suspensions were stained for multicolor analysis with the indicated fluorochrome- or
435 biotin-conjugated antibodies after blocking with Fc block (purified anti-CD16/32). Antibodies
436 were diluted in flow cytometry buffer (DPBS, 2% FCS) and staining was performed for 30 min on
437 ice in the dark. LIVE/DEAD™ Fixable Near-IR Dead Cell Stain Kit (Invitrogen), Fixable Viability Dye
438 eFluor™-780 (Invitrogen) or DRAQ7 (BioLegend) were used for determining the viability of cells.
439 Lymphocytes from *C. rodentium* infection experiments were treated with rmIL-23 (40 ng/ml,
440 R&D) for 3 hours at 37°C with 5% CO_2, washed and further incubated with rmIL-23 (40 ng/ml),
441 PMA (50 ng/ml, Sigma Aldrich), Ionomycin (750 ng/ml, Sigma Aldrich) and BD GolgiStop™
442 (containing monensin at 1:1000 dilution, BD) for an additional 3.5 hours at 37 °C with 5% CO_2.
443 For intracellular staining, cells were fixed with the Foxp3 Fixation/Permeabilization kit from
444 eBioscience. Samples were acquired on a Fortessa X20, a LSRFortessa or a Symphony flow
445 cytometer (BD Biosciences) using FACSDiva software (BD Biosciences) and analyzed with
446 FlowJo software (Tree Star). The following antibodies were used: PE-Cy7/APC-Cy7 anti-mouse
447 NK1.1 (clone PK136), PE-Cy7/BUV737/APC-Cy7 anti-mouse CD3 (clone 145-2C11 or 17A2), PE-
448 Cy7/APC-Cy7 anti-mouse B220 (clone RA3-6B2), PE-Cy7/APC-Cy7 anti-mouse CD19 (clone
449 eBio1D3 or 6D5), PE-Cy7 anti-mouse CD64 (clone X54-5/7.1), APC-Cy7 anti-mouse TER119 (clone
450 TER-119), APC/BV711/PerCP-Cy5.5 anti-mouse CD11c (clone N418/HL3), FITC/BUV661 anti-
451 mouse MHC-II (clone M5/114.15.2), APC-Cy7/BUV737/FITC/APC-R700 anti-mouse CD11b (clone
452 M1/70), PE/BV421 anti-mouse XCR1 (clone ZET), BV421/BV786 anti-mouse CD103 (clone M290),

453 APC-Cy7 anti-mouse CD24 (clone M1/69), BV605 anti-mouse CD8α (clone 53-6.7), APC/PE anti-
454 73LR3 (clone 11F8), BUV395/V500 anti-mouse CD45 (clone 30-F11), PE-CF594 anti-mouse
455 CD172a (SIRPα) (clone P84), APC/PE-Cy7 anti-mouse ESAM (clone 1G8/ESAM), APC/PE anti-
456 mouse IRF4 (clone 3E4), PerCP eF710 anti-mouse IRF8 (clone V3GYWCH), PE anti-mouse Clec9a
457 (clone 7H11), FITC anti-mouse Vβ 5.1,5.2 (clone MR9-4), PerCp-Cy5.5 anti-mouse CD44 (clone
458 IM7), PE anti-mouse CD45.2 (clone 104), Alexa Fluor® 647 anti-human/mouse Bcl-6 (clone K112-
459 91), APC-Cy7 anti-mouse CD45.1 (clone A20), BUV395 anti-mouse CD4 (clone GK1.5), BV786 anti-
460 mouse IL-17A (clone TC11-18H10), FITC anti-mouse CD90.2 (clone 53-21), PerCP-Cy5.5 anti-
461 mouse IFNγ (clone XMG1.2), PE-eF610 anti-mouse RORγt (clone BD2), PE anti-mouse IL-22 (clone
462 1H8BWSR) , PE-Cy7 anti-mouse T-bet (clone 4B10), APC anti-mouse Foxp3 (clone FJK-16S), APC-
463 eF780 anti-mouse TCRβ (clone H57-597), biotin anti-mouse CXCR5 (clone L138D7), BV785 anti-
464 mouse CD4 (clone RM4-5), Pacific Blue™ anti-rat CD90/mouse CD90.1 (Thy-1.1) (clone OX-7),
465 PerCP/Cyanine5.5 anti-mouse CD19 (clone 6D5), PE-eFluor™ 610 anti-mouse CD279 (PD-1) (clone
466 J43), and streptavidin conjugated to BUV737 or APC.
467
468 **Splenic dendritic cell sorting and cDNA library preparation for RNA-seq**
469
470 Splenic DC were enriched using the Dynabeads Mouse DC Enrichment kit (Invitrogen) and sorted
471 on a BD FACS Melody to obtain cDC1 ($B220^{-}CD64^{-}CD3^{-}CD19^{-}NK1.1^{-}CD11c^{hi}MHCII^{+}XCR1^{+}$) and
472 cDC2 ($B220^{-}CD64^{-}CD3^{-}CD19^{-}NK1.1^{-}CD11c^{hi}MHCII^{+}CD11b^{+}XCR1^{-}$). Sorted cells (2-4x$10^{4}$ per
473 sample) were resuspended in 350 μl RNeasy Lysis Buffer (QIAGEN), and RNA was extracted using
474 the QIAGEN RNeasy Mini kit (QIAGEN). RNA was washed, treated with DNase I (QIAGEN), and
475 eluted per the manufacturer's instructions. RNA-seq libraries were prepared by
476 combining the Nugen Ovation RNA-seq system with NuGEN's Ovation RNA-Seq System V2
477 (NuGEN Technologies). The amplified libraries were purified using AMPure beads, quantified by
478 qPCR, and visualized on an Agilent Bioanalyzer using BioA DNA High sensitivity (Agilent). The
479 libraries were pooled equimolarly and run on a HiSeq 2500 as single end reads of
480 50 nucleotide length.
481

482 **RNA-sequencing data analysis**

483

484 Sequencing reads were mapped to the mouse reference genome (GRCm38.85/mm10) using the
485 STAR aligner (v2.7.6a)[58]. Alignments were guided by a Gene Transfer Format (Ensembl GTF
486 GRCm38.101). Read count tables were normalized based on their library size factors using
487 DESeq2 (v1.30.1)[59], and differential expression analysis was performed with a filter of
488 log2foldChange >1 and a p-adjust value < 0.01. For selected gene signatures (cDC1 and cDC2 or
489 ESAM^{hi} and ESAM^{lo} DC2s) the 100 DEGs with highest normalized count values were selected, out
490 of which then the top 50 genes with highest absolute log2FoldChange were depicted in
491 heatmaps. RNA-seq reads aligned to genes from the GENCODE gene annotation were counted
492 using Ensembl's BiomaRt-v2.46.3. Heatmap visualizations were done using pheatmap v1.0.12.
493 Downstream statistical analyses and plot generation were performed in the R environment
494 (v4.0.5).[60] The online tool Venny 2.1 was used for the drawing of the Venn plots.[61]
495 Package PlotMA was used for visualizing of gene expression changes from two different
496 conditions (parameters: alpha = 0.01, type =”ashr”).[62] Principal Component Analysis (PCA) plots
497 were drawn using PCAtools 2.2.0, with removeVar=0.01.[63] Volcano plots were drawn using the
498 function of ggpubr 0.4.0.[64] Gene Set Enrichment Analysis was performed using Gene Ontology R
499 package clusterProfiler 3.18.1 (category biological process) on DEGs obtained from DESeq2. The
500 p-values were adjusted using "BH" (Benjamini-Hochberg) correction and the cutoff was
501 0.01.[65] GO biological process terms were ranked by GeneRatio. The gene ratio is defined as the
502 number of genes associated with the term in DEGs divided by the number of DEGs. For KEGG
503 enrichment, DESeq2 derived DEGs were used.[66] Enrichments with a p-value from Fisher’s exact
504 test ≤ 0.05 were considered significant.

505

506 **Confocal Microscopy**

507

508 Spleen and mLNs were harvested, washed with cold DPBS and placed in 4% PFA for 12 hours,
509 followed by an overnight wash with PBS-XG (PBS + 5% FCS + 0.2% Triton-X100 + 0.01%
510 Thimerosal). Samples were embedded in warm 4% low melting agarose. 70-100µm sections were

511 cut using a vibratome and stored until use. Samples were incubated with primary antibodies in
512 500ul PBS-XG in a 24 well plate overnight at 4°C under constant agitation (120rpm), followed by
513 at least 6 hours of washing in 5ml PBS-XG. The following antibodies were used: BV421 anti-mouse
514 B220/CD45R (clone RA3-6B2), APC anti-mouse TLR3 (clone 11F8), Alexa Fluor® 488 anti-mouse
515 CD11c (clone N418) and PE-CF594 anti-mouse CD172a (SIRPα) (clone P84). Sections were
516 mounted using ProLong Gold and images were acquired on a Zeiss LSM710 confocal microscope
517 equipped with 488-, 561-, and 633-nm lasers and a tunable two-photon laser. Digital pictures at
518 1,024 × 1,024-pixel density and 8-bit depth were acquired with ZEN software (Zeiss).
519
520 **Cross-presentation assay**
521
522 Naïve CD8 T cells from OT-I donors were enriched using the Dynabeads® Untouched™ Mouse T
523 Cells kit (Invitrogen) and stained in 1ml DPBS with CellTrace Violet dye (Invitrogen) for 10 min
524 at 37°C. 1 x 10^6 OT-I cells were transferred into recipients one day before i.p. injection of 5 x
525 10^6 cells/mouse of H-$2^{\beta m1}$ MEFs expressing truncated non-secreted OVA (OVA-MEF).[17] One day
526 after immunization, recipients were injected with FTY720 (20 µg/mouse; Cayman) in saline i.p..
527 Mice were sacrificed three days after immunization.
528
529 **Induction of Tfh cells *in vivo***

530 For adoptive transfer experiments into *CD11c.Bcl6^{KO}* or control hosts, naïve $CD4^+$ T cells were
531 enriched from homozygous TCR-transgenic OT-II (CD45.1/.2) donors using the Dynabeads
532 Untouched™ Mouse CD4 Cells kit (Invitrogen). 1 x 10^5 OT-II cells were transferred intravenously
533 (i.v.) and one day later, recipients were immunized i.p. with ovalbumin grade V (OVA, 0.5 mg,
534 Sigma Aldrich) together with poly(I:C) (100 µg, Sigma-Aldrich). Controls received PBS alone and
535 mice were sacrificed three days after immunization. For adoptive transfer experiments into
536 *Clec9a.Bcl6^{CONTROL}* or *Clec9a.Bcl6^{KO}* hosts, naïve $CD4^+$ T cells were enriched from heterozygous
537 OT-II (Thy1.1) donors using the EasySep™ Mouse Naïve $CD4^+$ T Cell Isolation Kit (Stemcell
538 Technologies) according to the manufacturer's instructions. 2x10^5 OT-II cells were injected i.v.,
539 and one day later, recipient mice were immunized i.p. with a 1:1 mixture of 50 µg OVA (Sigma)

540 in PBS and Imject Alum (Thermo Fisher). Seven days later, spleens were dissected and analyzed
541 by flow cytometry.
542
543 ***Citrobacter rodentium* infection**
544
545 The *C. rodentium* strain DBS100 (ATCC 51459; American Type Culture Collection) was used as
546 described[67] with some amendments. Briefly, *C. rodentium* cultures were grown in Luria-Bertani
547 (LB) medium to an OD_{600} of 1-1.5. Mice were orally inoculated with LB broth or $2x10^9$ CFU *C.*
548 *rodentium*, and their weight was monitored daily. Fecal samples were collected on indicated days
549 post infection, serially diluted in PBS and plated on Brilliance™ E. coli/coliform Agar (Thermo
550 Fisher). *C. rodentium* colonies, from at least three dilutions per sample, were enumerated and
551 normalized to weight of feces.

552 For histopathology, 0.5 cm of the distal colon was immediately placed in 10% formalin and
553 processed by the DTU Histology Core for hematoxylin and eosin (H&E) staining. Images were
554 acquired on a Pannoramic MIDI II scanner (3DHISTECH) and visualized with CaseViewer software
555 2.4 (3DHISTECH). The severity of the infection was assessed in a blinded manner.

556
557 **Statistical Analysis**
558
559 Statistical analyses were performed with Graphpad Prism 9.0 (Graphpad Software).
560

561

562 **Supplementary Materials**

563 Supplementary Figure 1: Phenotype and abundance of lung and blood cDC lacking Bcl6

564 Supplementary Figure 2: Quantification of spleen cDC in *Clec9a.Bcl6*^{KO} mice

565 Supplementary Figure 3: Intracellular Foxp3 and cytokine staining of colonic CD4+ T cells from
566 *Citrobacter rodentium* infected mice

567

568 Supplementary Table 1: Expression levels of top 50 DEGs between control cDC1 and control cDC2

569 Supplementary Table 2: DEGs between control and *XCR.Bcl6*^{KO} cDC1 and control and
570 *CD11c.Bcl6*^{KO} cDC2

571 Supplementary Table 3: Expression levels of top 50 DEGs between ESAM^{hi} and ESAM^{lo} cDC2

572

573 **References**

574 1. Guilliams, M. *et al.* Dendritic cells, monocytes and macrophages: a unified nomenclature
575 based on ontogeny. *Nat. Rev. Immunol.* **14**, 571–578 (2014).

576 2. Steinman, R. M. the Dendritic Cell System. *Annu. Rev. Immunol.* **9**, 271–296 (1991).

577 3. Durai, V. & Murphy, K. M. Functions of Murine Dendritic Cells. *Immunity* **45**, 719–736
578 (2016).

579 4. Allenspach, E. J., Lemos, M. P., Porrett, P. M., Turka, L. A. & Laufer, T. M. Migratory and
580 Lymphoid-Resident Dendritic Cells Cooperate to Efficiently Prime Naive CD4 T cells.
581 *Immunity* **29**, 795–806 (2008).

582 5. Lewis, S. M., Williams, A. & Eisenbarth, S. C. Structure and function of the immune
583 system in the spleen. *Sci. Immunol.* **4**, (2019).

584 6. Eisenbarth, S. C. Dendritic cell subsets in T cell programming: location dictates function.
585 *Nat. Rev. Immunol.* **19**, (2018).

586 7. Calabro, S. *et al.* Differential Intrasplenic Migration of Dendritic Cell Subsets Tailors
587 Adaptive Immunity. *Cell Rep.* **16**, 2472–2485 (2016).

588 8. Idoyaga, J., Suda, N., Suda, K., Park, C. G. & Steinman, R. M. Antibody to Langerin/CD207

589 localizes large numbers of CD8α + dendritic cells to the marginal zone of mouse spleen.
590 *Proc. Natl. Acad. Sci. U. S. A.* **106**, 1524–1529 (2009).

591 9. Sichien, D. *et al.* IRF8 Transcription Factor Controls Survival and Function of Terminally
592 Differentiated Conventional and Plasmacytoid Dendritic Cells, Respectively. *Immunity* **45**,
593 626–640 (2016).

594 10. Schiavoni, G. *et al.* ICSBP is essential for the development of mouse type I interferon-
595 producing cells and for the generation and activation of CD8α+ dendritic cells. *J. Exp.*
596 *Med.* **196**, 1415–1425 (2002).

597 11. Hildner, K. *et al.* Batf3 deficiency reveals a critical role for CD8alpha+ dendritic cells in
598 cytotoxic T cell immunity. *Science* **322**, 1097–1100 (2008).

599 12. Kashiwada, M., Pham, N. L. L., Pewe, L. L., Harty, J. T. & Rothman, P. B. NFIL3/E4BP4 is a
600 key transcription factor for CD8α+ dendritic cell development. *Blood* **117**, 6193–6197
601 (2011).

602 13. Bagadia, P. *et al.* An Nfil3–Zeb2–Id2 pathway imposes Irf8 enhancer switching during
603 cDC1 development. *Nat. Immunol.* **20**, 1174–1185 (2019).

604 14. Hacker, C. *et al.* Transcriptional profiling identifies Id2 function in dendritic cell
605 development. *Nat. Immunol.* **4**, 380–386 (2003).

606 15. Cerovic, V. *et al.* Lymph-borne CD8α+ dendritic cells are uniquely able to cross-prime
607 CD8+ T cells with antigen acquired from intestinal epithelial cells. *Mucosal Immunol.* **8**,
608 38–48 (2015).

609 16. Joeris, T. *et al.* Intestinal cDC1 drive cross-tolerance to epithelial-derived antigen via
610 induction of FoxP3+CD8+ Tregs. *Sci. Immunol.* **6**, (2021).

611 17. Sancho, D. *et al.* Identification of a dendritic cell receptor that couples sensing of necrosis
612 to immunity. *Nature* **458**, 899–903 (2009).

613 18. Ahrens, S. *et al.* F-actin is an evolutionarily conserved damage-associated molecular
614 pattern recognized by DNGR-1, a receptor for dead cells. *Immunity* **36**, 635–45 (2012).

615 19. Zhang, J.-G. *et al.* The dendritic cell receptor Clec9A binds damaged cells via exposed
616 actin filaments. *Immunity* **36**, 646–57 (2012).

617 20. Watchmaker, P. B. *et al.* Comparative transcriptional and functional profiling defines
618 conserved programs of intestinal DC differentiation in humans and mice. *Nat. Immunol.*
619 **15**, 98–108 (2014).

620 21. Tussiwand, R. *et al.* Klf4 Expression in Conventional Dendritic Cells Is Required for T
621 Helper 2 Cell Responses. *Immunity* **42**, 916–928 (2015).

622 22. Satpathy, A. T. *et al.* Notch2-dependent classical dendritic cells orchestrate intestinal
623 immunity to attaching-and-effacing bacterial pathogens. *Nat Immunol* **14**, 937–948
624 (2013).

625 23. Persson, E. K. *et al.* IRF4 transcription-factor-dependent CD103(+)CD11b(+) dendritic cells
626 drive mucosal T helper 17 cell differentiation. *Immunity* **38**, 958–69 (2013).

627 24. Williams, J. W. *et al.* Transcription factor IRF4 drives dendritic cells to promote Th2
628 differentiation. *Nat Commun* **4**, 2990 (2013).

629 25. Scott, C. L. *et al.* The transcription factor Zeb2 regulates development of conventional
630 and plasmacytoid DC by repressing Id2. *J. Exp. Med.* jem.20151715 (2016).
631 doi:10.1084/jem.20151715

632 26. Ichikawa, E. *et al.* Defective development of splenic and epidermal CD4+ dendritic cells in
633 mice deficient for IFN regulatory factor-2. *Proc. Natl. Acad. Sci. U. S. A.* **101**, 3909–14
634 (2004).

635 27. Wu, L. *et al.* RelB is essential for the development of myeloid-related CD8alpha- dendritic
636 cells but not of lymphoid-related CD8alpha+ dendritic cells. *Immunity* **9**, 839–47 (1998).

637 28. Lewis, K. L. *et al.* Notch2 receptor signaling controls functional differentiation of dendritic
638 cells in the spleen and intestine. *Immunity* **35**, 780–791 (2011).

639 29. Briseño, C. G. *et al.* Notch2-dependent DC2s mediate splenic germinal center responses.
640 *Proc. Natl. Acad. Sci. U. S. A.* **115**, 10726–10731 (2018).

641 30. Fasnacht, N. *et al.* Specific fibroblastic niches in secondary lymphoid organs orchestrate
642 distinct Notch-regulated immune responses. *J. Exp. Med.* **211**, 2265–2279 (2014).

643 31. Caton, M. L., Smith-Raska, M. R. & Reizis, B. Notch–RBP-J signaling controls the
644 homeostasis of CD8 − dendritic cells in the spleen . *J. Exp. Med.* **204**, 1653–1664 (2007).

645 32. Lu, E., Dang, E. V., McDonald, J. G. & Cyster, J. G. Distinct oxysterol requirements for
646 positioning naïve and activated dendritic cells in the spleen. *Sci. Immunol.* **2**, eaal5237
647 (2017).

648 33. Choi, J. & Crotty, S. Bcl6-Mediated Transcriptional Regulation of Follicular Helper T cells
649 (TFH). *Trends Immunol.* **42**, 336–349 (2021).

650 34. Ohtsuka, H. *et al.* Bcl6 Is Required for the Development of Mouse CD4+ and CD8 +
651 Dendritic Cells. *J. Immunol.* **186**, 255–263 (2011).

652 35. Bagadia, P. *et al.* Bcl6 -Independent In Vivo Development of Functional Type 1 Classical
653 Dendritic Cells Supporting Tumor Rejection . *J. Immunol.* ji1901010 (2021).
654 doi:10.4049/jimmunol.1901010

655 36. Schraml, B. U. *et al.* Genetic tracing via DNGR-1 expression history defines dendritic cells
656 as a hematopoietic lineage. *Cell* **154**, 843–858 (2013).

657 37. Lau, C. M. *et al.* Leukemia-associated activating mutation of Flt3 expands dendritic cells
658 and alters T cell responses. *J. Exp. Med.* **213**, 415–431 (2016).

659 38. Baumjohann, D., Okada, T. & Ansel, K. M. Cutting Edge: Distinct Waves of BCL6
660 Expression during T Follicular Helper Cell Development. *J. Immunol.* **187**, 2089–2092
661 (2011).

662 39. Goenka, R. *et al.* Cutting Edge: Dendritic Cell-Restricted Antigen Presentation Initiates the
663 Follicular Helper T Cell Program but Cannot Complete Ultimate Effector Differentiation. *J.*
664 *Immunol.* **187**, 1091–1095 (2011).

665 40. Baumjohann, D. *et al.* Persistent Antigen and Germinal Center B Cells Sustain T Follicular
666 Helper Cell Responses and Phenotype. *Immunity* **38**, 596–605 (2013).

667 41. Zhang, S. *et al.* Type 1 conventional dendritic cell fate and function are controlled by DC-
668 SCRIPT. *Sci. Immunol.* **6**, (2021).

669 42. Zhang, T. T. *et al.* Dynamic expression of BCl6 in murine conventional dendritic cells
670 during in vivo development and activation. *PLoS One* **9**, 1–12 (2014).

671 43. Durai, V. *et al.* Cryptic activation of an Irf8 enhancer governs cDC1 fate specification. *Nat.*
672 *Immunol.* **20**, 1161–1173 (2019).

673 44. Grajales-Reyes, G. E. *et al.* Batf3 maintains autoactivation of Irf8 for commitment of a
674 CD8α+ conventional DC clonogenic progenitor. *Nat. Immunol.* **16**, 708–717 (2015).

675 45. Seillet, C. *et al.* Nfil3 is required for the development of all innate lymphoid cell subsets.
676 *J. Exp. Med.* **211**, 1733–40 (2014).

677 46. Kusunoki, T. *et al.* TH2 dominance and defective development of a CD8+ dendritic cell
678 subset in Id2-deficient mice. *J. Allergy Clin. Immunol.* **111**, 136–142 (2003).

679 47. Dudziak, D. *et al.* Differential antigen processing by dendritic cell subsets in vivo. *Science*
680 **315**, 107–11 (2007).

681 48. Gatto, D. *et al.* The chemotactic receptor EBI2 regulates the homeostasis, localization
682 and immunological function of splenic dendritic cells. *Nat. Immunol.* **14**, 446–453 (2013).

683 49. Yi, T. & Cyster, J. G. EBI2-mediated bridging channel positioning supports splenic
684 dendritic cell homeostasis and particulate antigen capture. *Elife* **2**, e00757 (2013).

685 50. Huang, C. *et al.* The BCL6 RD2 Domain Governs Commitment of Activated B Cells to Form
686 Germinal Centers. *Cell Rep.* **8**, 1497–1508 (2014).

687 51. Schlitzer, A. *et al.* IRF4 transcription factor-dependent CD11b+ dendritic cells in human
688 and mouse control mucosal IL-17 cytokine responses. *Immunity* **38**, 970–83 (2013).

689 52. Kedmi, R. *et al.* A RORγt+ cell instructs gut microbiota-specific Treg cell differentiation.
690 *Nature* (2022). doi:10.1038/s41586-022-05089-y

691 53. Crotty, S., Johnston, R. J. & Schoenberger, S. P. Effectors and memories: Bcl-6 and Blimp-

692 1 in T and B lymphocyte differentiation. *Nat Immunol* **11**, 114–120 (2010).

693 54. Wohn, C. *et al.* Absence of MHC class II on cDC1 dendritic cells triggers fatal
694 autoimmunity to a cross-presented self-antigen. *Sci. Immunol.* **5**, (2020).

695 55. Hollister, K. *et al.* Insights into the Role of Bcl6 in Follicular Th Cells Using a New
696 Conditional Mutant Mouse Model. *J. Immunol.* **191**, 3705–3711 (2013).

697 56. Baumjohann, D. & Ansel, K. M. Tracking Early T Follicular Helper Cell Differentiation In
698 Vivo. in *Methods in molecular biology* **1291**, 27–38 (2015).

699 57. Johansson-Lindbom, B. *et al.* Functional specialization of gut CD103 + dendritic cells in
700 the regulation of tissue-selective T cell homing . *J. Exp. Med.* **202**, 1063–1073 (2005).

701 58. Dobin, A. *et al.* STAR: Ultrafast universal RNA-seq aligner. *Bioinformatics* **29**, 15–21
702 (2013).

703 59. Love, M. I., Huber, W. & Anders, S. Moderated estimation of fold change and dispersion
704 for RNA-seq data with DESeq2. *Genome Biol.* **15**, (2014).

705 60. R Core Team (2020). R: A language and environment for statistical computing. R
706 Foundation for Statistical Computing, Vienna, Austria. (2020).

707 61. Oliveros, J. C. Venny. An Interactive Tool for Comparing Lists with Venn's Diagrams.

708 62. Stephens, M. False discovery rates: A new deal. *Biostatistics* **18**, 275–294 (2017).

709 63. Blighe, K. and A. L. PCAtools: everything Principal Components
710 Analysis.https://github.com/kevinblighe/PCAtools. (2019).

711 64. Alboukadel Kassambara. ggpubr:'ggplot2' Based Publication Ready Plots. (2020).

712 65. Yu, G., Wang, L.-G., Han, Y. & He, Q.-Y. clusterProfiler: an R Package for Comparing
713 Biological Themes Among Gene Clusters. *Omi. A J. Integr. Biol.* **16**, (2012).

714 66. Qiu, Y.-Q. KEGG Pathway Database. in *Encyclopedia of Systems Biology* (eds. Dubitzky,
715 W., Wolkenhauer, O., Cho, K.-H. & Yokota, H.) 1068–1069 (Springer New York, 2013).
716 doi:10.1007/978-1-4419-9863-7_472

717 67. Rizk, J. *et al.* The cIAP ubiquitin ligases sustain type 3 γδ T and innate lymphoid cells
718 during aging to allow normal cutaneous and mucosal responses. *bioRxiv* (2022).
719 doi:10.1101/2020.05.14.094334

720

721 **Acknowledgements**

722 We thank Katrine Fog Starup and Julien Vandamme for excellent technical support, the Lahl,
723 Agace and Bekiaris laboratories for fruitful discussions, and Prof Allan Mowat for intellectual
724 input and manuscript editing. *Bcl6*$^{fl/fl}$ mice were kindly gifted by Alexander Dent and the OVA-
725 MEF line was from Caetano Reis e Sousa. H&E sections were processed by Susanne Primdahl and
726 histology data was generated using research infrastructure at DTU National Food Institute,
727 including FOODHAY (Food and Health Open Innovation Laboratory, Danish Roadmap for
728 Research Infrastructure).

729

730 **Funding**

731 This study was funded by the China Scholarship Council fellowship (HX), a Lundbeck Foundation
732 Fellowship R215-2015-4100, the Ragnar Söderberg Foundation Fellowship in Medicine,
733 Vetenskapsrådet 2020-01977, Cancerfonden 21 1826 Pj, the Novo Nordisk Foundation 18038,
734 and the Crafoord Foundation (all KL), the European Research Council ERC-2016-STG-715182,
735 Deutsche Forschungsgemeinschaft (DFG, German Research Foundation) Emmy Noether grant
736 Schr 1444/1-1, Project-ID 360372040 – SFB 1335 (project 8) and 322359157-FOR2599-A03 (all
737 BS), the Deutsche Forschungsgemeinschaft (DFG, German Research Foundation) Emmy Noether
738 Programme BA 5132/1-2 (252623821), an SFB 1054 Project B12 (210592381) (DB) and Germany's
739 Excellence Strategy EXC2151 (390873048) (all to DB) and by the Deutsche
740 Forschungsgemeinschaft (DFG, German Research Foundation) under Germany's Excellence
741 Strategy – EXC2151 – 390873048 (AS), an Emmy Noether research grant (SCHL2116/1-1 to AS),
742 the CRC1454 - INST 217/1034-1(Subproject P05) and a DFG Research Grant (SCHL2116/6-1) to
743 AS.

744

745 **Author Contributions:**

746 Conceptualization: KL

747 Methodology: HX, IU, JH, HN, LB, IK, UM, LZ, AS, FP, BS, DB, KL
748 Investigation: HX, IU, JH, HN, LB, IK, UM, LZ, BS, DB, KL
749 Visualization: HX, IU, UM, KL
750 Funding acquisition: HX, DB, BS, KL
751 Project administration: KL
752 Supervision: FP, AS, BS, DB, KL
753 Writing – original draft: KL
754 Writing – review & editing: IU, BS, DB, KL
755

756 **Competing Interests**

757 The authors declare that they have no competing interests.

758

759 **Data Availability**

760 Raw RNA-sequencing data files are accessible through the NCBI SRA database under the
761 accession number PRJNA834905.

762

763 **Figures:**

764 **Fig. 1: Phenotype and abundance of lymphoid tissue resident cDC lacking Bcl6**

765 A. Left: Splenic XCR1^{+} and XCR1^{-}CD11b^{+} DC subsets in control (black), *XCR1.Bcl6^{KO}* (orange), and
766 *CD11c.Bcl6^{KO}* (red) mice. Plots show representative staining profiles of gated live, single lineage^{-}
767 (CD3, CD19, CD64, B220, NK1.1), MHCII^{+}, CD11c^{hi} splenocytes. Right: Absolute numbers of splenic
768 XCR1^{+} and XCR1^{-}CD11b^{+} DC from control, *XCR1.Bcl6^{KO}*, and *CD11c.Bcl6^{KO}* mice. Statistical analysis
769 by one-way ANOVA. * P<0.01 and ** P<0.001. Data points represent values from individual mice
770 pooled from 8-9 experiments and lines represent the medians.
771 B. Left: Flow cytometry plots showing resident XCR1^{+} and XCR1^{-}CD11b^{+} DC subsets in the pLNs and
772 mLNs of control, *XCR1.Bcl6^{KO}*, and *CD11c.Bcl6^{KO}* mice. Plots show representative staining profiles
773 of gated single live, CD45^{+}, lineage^{-} (CD3, CD19, CD64, B220, NK1.1), CD11c^{hi}MHCII^{int} resident DC.
774 Right: Absolute numbers of resident cDC subsets in the pLN and mLN of control, *XCR1.Bcl6^{KO}*, and

775 *CD11c.Bcl6^{KO}* mice. Statistical analysis by one-way ANOVA. * P<0.05. Data points represent values
776 from individual mice pooled from at least four experiments and lines represent the medians.

777

778 **Fig. 2: Phenotype and abundance of migratory cDC subsets lacking Bcl6**

779 A. Left: Flow cytometry plots showing migratory XCR1^{+} and XCR1^{-}CD11b^{+} DC subsets in the pLN (top)
780 and mLN (middle) of control (black), *XCR1.Bcl6^{KO}* (orange), and *CD11c.Bcl6^{KO}* (red) mice. mLN
781 XCR1^{-} DC are further sub-divided into CD103^{+} and CD103^{-} (bottom). Plots show representative
782 staining profiles of live single, CD45^{+}, lineage^{-} (CD3, CD19, CD64, B220, NK1.1), CD11c^{int}MHCII^{hi}
783 migratory DC. Right: Absolute numbers of migratory cDC subsets from pLN and mLN of control,
784 *XCR1.Bcl6^{KO}*, and *CD11c.Bcl6^{KO}* mice. Statistical analysis by one-way ANOVA. * P<0.05, ** P<0.01,
785 *** P<0.001 and **** P<0.0001. Data points represent values from individual mice pooled from
786 at least four experiments and lines represent the medians.
787 B. Left: Flow cytometry plots showing SILP XCR1^{+} and XCR1^{-}CD11b^{+} DC subsets from control,
788 *XCR1.Bcl6^{KO}*, and *CD11c.Bcl6^{KO}* mice. Plots show representative staining profiles of live, CD45^{+},
789 lineage^{-} (CD3, CD19, CD64, B220, NK1.1), MHCII^{+}, CD11c^{hi} gated single cells.
790 Right: Absolute numbers of XCR1^{+} and XCR1^{-}CD11b^{+} DC subsets from control, *XCR1.Bcl6^{KO}*, and
791 *CD11c.Bcl6^{KO}* mice. Statistical analysis was performed by one-way ANOVA.* P<0.05 and ** P<0.01.
792 Data points represent values from individual mice pooled from three experiments and lines
793 represent the medians.

794

795 **Fig. 3: Lineage identity of splenic Bcl6-deficient cDC subsets**

796 A. Principal component analysis (PCA) plot of gene expression data obtained from bulk RNA-seq
797 using DESeq2. Color coded icons show cDC1 and cDC2 from the spleen of control, *XCR1.Bcl6^{KO}*,
798 and *XCR1.Bcl6^{KO}* mice. Three replicates were included in each group.
799 B. Heatmap of selected highly expressed cDC1 or cDC2 associated genes in all RNA-Seq samples (50
800 most differentially expressed genes between cDC1 and cDC2 chosen from the 100 genes with
801 highest expression level among total differentially expressed genes (fold change $\geqslant$ 2, padj: 0.01)
802 in control samples). The color scale represents the row Z score.
803 C. Volcano plots showing the global transcriptional differences between splenic cDC2 and cDC1 in
804 control (left), *XCR1.Bcl6^{KO}* (middle) and *CD11c.Bcl6^{KO}* mice (right). Each circle represents one gene.

The log2FoldChange (LFC) is represented on the x-axis. The y-axis shows the –(log10 of the p adjust value). A padj value of 0.01 and an absolute LFC of 1 are indicated by dashed lines. The upregulated or downregulated genes are shown in red or blue dots respectively, and the top ranked gene symbols with the lowest padj value were annotated in the plot.

D. VENN diagram showing significantly elevated differentially expressed genes (DEGs) (|Log2foldchange|⩾1 and padj<0.01) between *XCR1.Bcl6*^{KO} cDC1 (red) and control cDC1 (blue), and between *CD11c.Bcl6*^{KO} cDC2 (orange) and control cDC2 (green).

Fig. 4: Phenotype and gene expression profiles of Bcl6-deficient splenic cDC1

A. Flow cytometric analysis of cDC1 in spleen of control and *XCR1.Bcl6*^{KO} mice. Representative histograms show indicated protein expression by control (black) and *XCR1.Bcl6*^{KO} (red) cDC1, with FMO staining shown in grey. Pre-gating on cDC1 was performed as in 1A. Data are representative of two independent experiments with 2-3 mice each.

B. Gene ontology (GO) term enrichment analysis of differentially expressed genes (DEGs) in *XCR1.Bcl6*^{KO} and control cDC1. The p value calculated from GO term enrichment analysis is represented on the x-axis and the y-axis shows the GO Biological Process (BP) terms.

C. KEGG (Kyoto Encyclopedia of Genes and Genomes) term enrichment analysis of DEGs in *XCR1.Bcl6*^{KO} vs control cDC1. The GeneRatio value calculated from KEGG term enrichment analysis is represented on the x-axis and the y-axis shows the KEGG enriched terms.

D. Heatmap of all genes contributing to the enriched KEGG pathways depicted in B. The color scale represents the row Z score.

Fig. 5: Cross-presentation by cDC1 deficient in Bcl6

A. Representative flow cytometry plots showing CTV dilution and CD44 expression on OT-I cells (gated on live, CD3^{+}CD8^{+}CD45.1^{+} single cells) in the spleen (top) and mLN (bottom) of control and *XCR1.Bcl6*^{KO} recipient mice three days after i.p. immunization with heat-shocked OVA-MEFs. Data are representative of three independent experiments with 2-5 mice each.

B. Total number of OT I cells in the spleen (right) and mLN (left) of immunized control and *XCR1.Bcl6*^{KO} mice. Data are pooled from three independent experiments. Each dot represents one mouse and lines represent the medians. Statistical analysis using Mann-Whitney test, *p<0.05.

835

836 **Fig. 6: Phenotype and gene expression profiles of splenic Bcl6-deficient cDC2**

837 A. Representative flow cytometric analysis of cDC2 in the spleen of control and *CD11c.Bcl6^{KO}* mice,
838 showing expression of CD11c vs MHCII (top panels) and XCR1 vs CD11b (lower panels) by live,
839 lineage^{-} (CD3, CD19, CD64, B220, NK1.1) single cell-gated splenocytes. Data are representative of
840 at least 8 independent experiments with 1 – 3 mice each.
841 B. Representative flow cytometric analysis of ESAM^{hi} and ESAM^{lo} cDC2 in the spleen of control and
842 *CD11c.Bcl6^{KO}* mice. Cells were pre-gated as XCR1^{-}CD11b^{+} cDC2 from live, lineage^{-} (CD3, CD19,
843 CD64, B220, NK1.1) single cells. Data are representative of three independent experiments with
844 1 – 3 mice each.
845 C. Representative flow cytometric analysis of cDC2 in the spleen of control and *Clec9a.Bcl6^{KO}* mice,
846 showing expression of CD11c vs MHCII (top panels) and XCR1 vs CD11b (lower panels) by live,
847 lineage^{-} (CD3, CD19, CD64, B220, NK1.1) single cell-gated splenocytes. Data are representative of
848 two independent experiments with 3 mice each.
849 D. Representative flow cytometric analysis of ESAM^{hi} and ESAM^{lo} cDC2 in the spleen of control and
850 *Clec9a.Bcl6^{KO}* mice. Cells were pre-gated as XCR1^{-}CD11b^{+} cDC2 from live, lineage^{-} (CD3, CD19,
851 CD64, B220, NK1.1) single cells (top). Data are representative of two independent experiments
852 with 3 mice each.
853 E. Same data as in D, but pre-gated on YFP^{+} cells to enrich for cDC2 with a history of Clec9A-promoter
854 activity.
855 F. Representative flow cytometric analysis of expression of CD11c, 33D1, CD4, CD11b and IRF4 by
856 splenic XCR1^{-}CD11b^{+} cDC2 from control (ESAM^{hi}: black, ESAM^{lo}: blue) or *CD11c.Bcl6^{KO}* mice
857 (orange). FMO controls are depicted in gray. Gates correspond to those depicted in Fig. 6B. Results
858 are representative of at least two (CD11c) or three (all others) independent experiments with 3
859 mice each.
860

861 **Fig. 7: Consequences for germinal center reactions caused by Bcl6 deficiency in splenic cDC**

862 A. Gene set enrichment plots following *CD11c.Bcl6^{KO}* vs control cDC2 in an ESAM^{hi} cDC2 related gene
863 set (top) vs an ESAM^{lo} cDC2 related gene set (bottom) (ESAM^{hi} and ESAM^{lo} gene sets derived from
864 GSE76132). NES = normalized enrichment score. FDR q-value: 0.0.

865 B. The top 50 genes associated with spleen ESAM^{hi} cDC2 (left) or ESAM^{lo} cDC2 (right) were derived
866 from GSE76132. Heatmaps show the expression of these genes in the RNA-Seq analysis of cDC2
867 from control and *CD11c.Bcl6^{KO}* spleen. The color scale represents the row Z score (Expression Z-
868 scale).
869 C. Confocal microscopy of spleens from *CD11c.Bcl6^{KO}* and control mice showing expression of TLR3
870 (grey: upper left quadrant), CD11c (green: upper right quadrant), Sirpα (red: lower left quandrant)
871 and B220 (blue: lower right quadrant). Scale bar=50μm. Orange arrows indicate marginal zone
872 bridging channels. The images shown are from one out of four (*CD11c.Bcl6^{KO}*) or three (control)
873 replicates derived from individual mice.
874 D. Schematic depiction of immunization schedules.
875 E. Top: Representative flow cytometric analysis of early Tfh cell induction amongst OT-II cells in the
876 spleen of control and *CD11c.Bcl6^{KO}* mice 3 days after i.p. immunization with OVA and poly(I:C) or
877 with PBS as a control. Tfh were gated as live, CD4$^+$Vβ5.2$^+$CD45.1$^+$CD45.2$^+$CD44$^+$Bcl6$^+$CXCR5$^+$ and
878 the results are representative of three experiments with 3-5 mice each. Each experiment
879 contained at least one unimmunized (PBS) control per genotype. Bottom: Numbers of total CD44$^+$
880 OT-II T cells (left panel), together with absolute numbers (middle panel) and proportions (right
881 panel) of OVA-specific Tfh cells in the spleens of control and *CD11c.Bcl6^{KO}* mice 3 days after i.p.
882 immunization with OVA and poly(I:C) or with PBS as a control. Statistical analysis was performed
883 by one-way ANOVA. * P<0.05, ** P<0.01, *** P<0.001 and **** P<0.0001. Data points represent
884 values from individual mice pooled from three experiments with 3-5 mice each in OVA/poly(I:C)
885 immunized groups. Each experiment contained at least one untreated control per genotype; lines
886 represent the medians.
887 F. Representative flow cytometric analysis of splenic OT-II cells transferred into *Clec9a.Bcl6^{CONTROL}*
888 and *Clec9a.Bcl6^{KO}* recipients 7 days after i.p. immunization with OVA/alum. Tfh cells were gated
889 as CXCR5$^+$PD-1$^+$ cells among live CD4$^+$Thy1.2$^+$CD19$^-$ lymphocytes. Statistical analysis was
890 performed by Mann-Whitney test, ** P<0.01. Each symbol represents one biological replicate
891 (n=5), lines represent the median. Data are representative of two independent experiments.
892

893 **Fig. 8: *Citrobacter rodentium* infection in mice with Bcl6 deletion in cDC**

894 A. Left: Flow cytometry plots showing cLP XCR1$^+$ and XCR1$^-$CD11b$^+$ DC subsets gated on all DC (live,
895 CD45$^+$, lineage$^-$ (CD3, CD19, CD64, B220, NK1.1), MHCII$^+$, CD11c^{hi} single cells. Right: XCR1$^-$ DC are
896 further sub-divided into CD103$^+$ and CD103$^-$ cDC2s from control and *CD11c.Bcl6^{KO}* mice.
897 B. Absolute numbers (top) and proportions (bottom) of cLP XCR1$^+$, XCR1$^-$CD103$^+$CD11b$^+$ and XCR1$^-$
898 CD103$^-$CD11b$^+$ DC subsets from control and *CD11c.Bcl6^{KO}* mice. Data points represent values from
899 individual mice pooled from 3 experiments and lines represent the medians. Statistical analysis
900 using Mann-Whitney test, ** P<0.01 and *** P<0.001.
901 C. Percentage of weight loss of mock and *C. rodentium* infected control and *CD11c.Bcl6^{KO}* mice. Each
902 symbol represents the mean weight loss of all mice within the group at the indicated time point
903 post infection versus their starting weight and error bars represent SD; statistical analysis using
904 two-way ANOVA (and Tukey's multiple comparison test) with Geisser-Greenhouse correction, *P
905 < 0.05 and **P < 0.01 (top left). Colon lengths in mock and infected mice at 9 or 21 days post
906 inoculation; statistical analysis by one-way ANOVA, ** P<0.01, **** P<0.0001 (bottom left). *C.*
907 *rodentium* titers in feces measured as colony-forming units (CFU) of infected control and
908 *CD11c.Bcl6^{KO}* mice at indicated days post infection; statistical analysis using Mann-Whitney test,
909 not significant (right). All data points represent values from individual mice, lines represent the
910 median and data is pooled from 2-3 experiments with 3-5 mice per mock/*C. rodentium* infected
911 group.
912 D. H&E-stained sections of the distal colon of mock and *C. rodentium* infected control and
913 *CD11c.Bcl6^{KO}* mice 21 days post inoculation. Scale bar, 100 µm. Symbols: # epithelial lining; ¤
914 leukocyte infiltration; % goblet cell destruction; & villus length. Representative of 4-5 mice per
915 group from one experiment.
916 E. Numbers of total CD4$^+$ T cells, IL-17A$^+$IL-22$^-$, IL-17A$^+$IL-22$^+$, IL-17A$^+$IFNγ$^-$, IL-17A$^+$IFNγ$^+$ and Foxp3$^+$
917 CD4$^+$ T cells in the cLP of mock and *C. rodentium* infected control and *CD11c.Bcl6^{KO}* mice at day 9
918 post inoculation. Statistical analysis performed by one-way ANOVA, * P<0.05, ** P<0.01, ***
919 P<0.001 and **** P<0.0001.
920 F. Numbers of total CD4$^+$ T cells, IL-17A$^+$IL-22$^-$, IL-17A$^+$IL-22$^+$, IL-17A$^+$IFNγ$^-$, IL-17A$^+$IFNγ$^+$ and Foxp3$^+$
921 T cells in the cLP of mock and *C. rodentium* infected control and *CD11c.Bcl6^{KO}* mice at day 21 post
922 inoculation. * P<0.05, ** P<0.01 and **** P<0.0001, by one-way ANOVA.

923

924 **Supplementary Figure 1**

925 A. Left: Flow cytometry plots show XCR1$^+$ and XCR1$^-$CD11b$^+$ DC subsets in the lungs of control,
926 *XCR1.Bcl6^{KO}* and *CD11c.Bcl6^{KO}* mice. The plots show representative staining profiles of live, CD45$^+$,
927 lineage$^-$ (CD3, CD19, CD64, B220, NK1.1), MHCII$^+$, CD11c^{hi} gated single cells. Right: Absolute
928 numbers of cDC subsets in the lungs of control, *XCR1.Bcl6^{KO}*, and *CD11c.Bcl6^{KO}* mice. Statistical
929 analysis by one-way ANOVA.** P<0.01, **** P<0.0001. Data points represent values from
930 individual mice pooled from 2-3 experiments and lines represent the medians.
931 B. Left: Representative flow cytometry plots of blood XCR1$^+$ and XCR1$^-$CD11b$^+$ DC subsets from
932 control, XCR1.Bcl6^{KO} and CD11c.Bcl6^{KO}. Shown are representative staining profiles of live, CD45$^+$,
933 lineage$^-$ (CD3, CD19, CD64, B220, NK1.1), MHCII$^+$, CD11c^{hi} gated single cells. Right: Absolute
934 numbers of cDC1 and cDC2 in blood of control, XCR1.Bcl6^{KO}, and CD11c.Bcl6^{KO} mice. Statistical
935 analysis by one-way ANOVA, significance at * P<0.05. Data points are normalized to volume of
936 blood drawn and represent values from individual mice pooled from 4 experiments; lines
937 represent the median cell numbers from each genotype.

938

939 **Supplementary Figure 2**

940 A. Relative proportions of XCR1$^+$, XCR1$^-$CD11b$^+$ESAM^{hi} and XCR1$^-$CD11b$^+$ESAM^{lo} subsets in the spleen
941 of Clec9a.*Bcl6^{KO}* (top) and CD11c.*Bcl6^{KO}* (bottom) mice. Cells were pre-gated on single live, CD45$^+$,
942 lineage$^-$ (CD3, CD19, TER119, B220, NK1.1), MHCII$^+$, CD11c^{hi}. Data points represent values from
943 individual mice pooled from 2-3 experiments and lines represent the medians. Statistical analysis
944 using Mann-Whitney test, *** P<0.001 and **** P<0.0001.
945 B. Numbers of XCR1$^+$, XCR1$^-$CD11b$^+$ESAM^{hi} and XCR1$^-$CD11b$^+$ESAM^{lo} subsets in the spleen of control,
946 Clec9a.*Bcl6^{KO}* normalized to volume of suspension (top) and CD11c.*Bcl6^{KO}* shown as absolute
947 numbers (bottom). Data points represent values from individual mice pooled from 2-3
948 experiments and lines represent the medians. * P<0.05, *** P<0.001 and **** P<0.0001, by
949 Mann-Whitney test.

950

951 **Supplementary Figure 3**

952 A. Representative flow cytometry plots showing Foxp3$^+$ CD4$^+$ T cells (gated on live, CD45$^+$,
953 CD3$^+$TCRβ$^+$ singlets) in the cLP of mock and *C. rodentium* infected control and *CD11c.Bcl6^{KO}* mice
954 at day 9 (left) or day 21 (right) post inoculation.

955 B. Representative flow cytometry analysis showing IL-17A$^+$IL-22$^+$ CD4$^+$ T cells (gated on live, CD45$^+$,
956 CD3$^+$TCRβ$^+$ singlets) in the cLP of mock and *C. rodentium* infected control and *CD11c.Bcl6^{KO}* mice
957 at day 9 (left) or day 21 (right) post inoculation.
958 C. Representative flow cytometry plots showing IL-17A$^+$IFNγ$^+$ CD4$^+$ T cells (gated on live, CD45$^+$,
959 CD3$^+$TCRβ$^+$ singlets) in the cLP of mock and *C. rodentium* infected control and *CD11c.Bcl6^{KO}* mice
960 at day 9 (left) or day 21 (right) post inoculation.
961
962
963
964
965
966
967
968
969
970
971
972
973
974
975
976
977
978
979

980 **Figure 1**

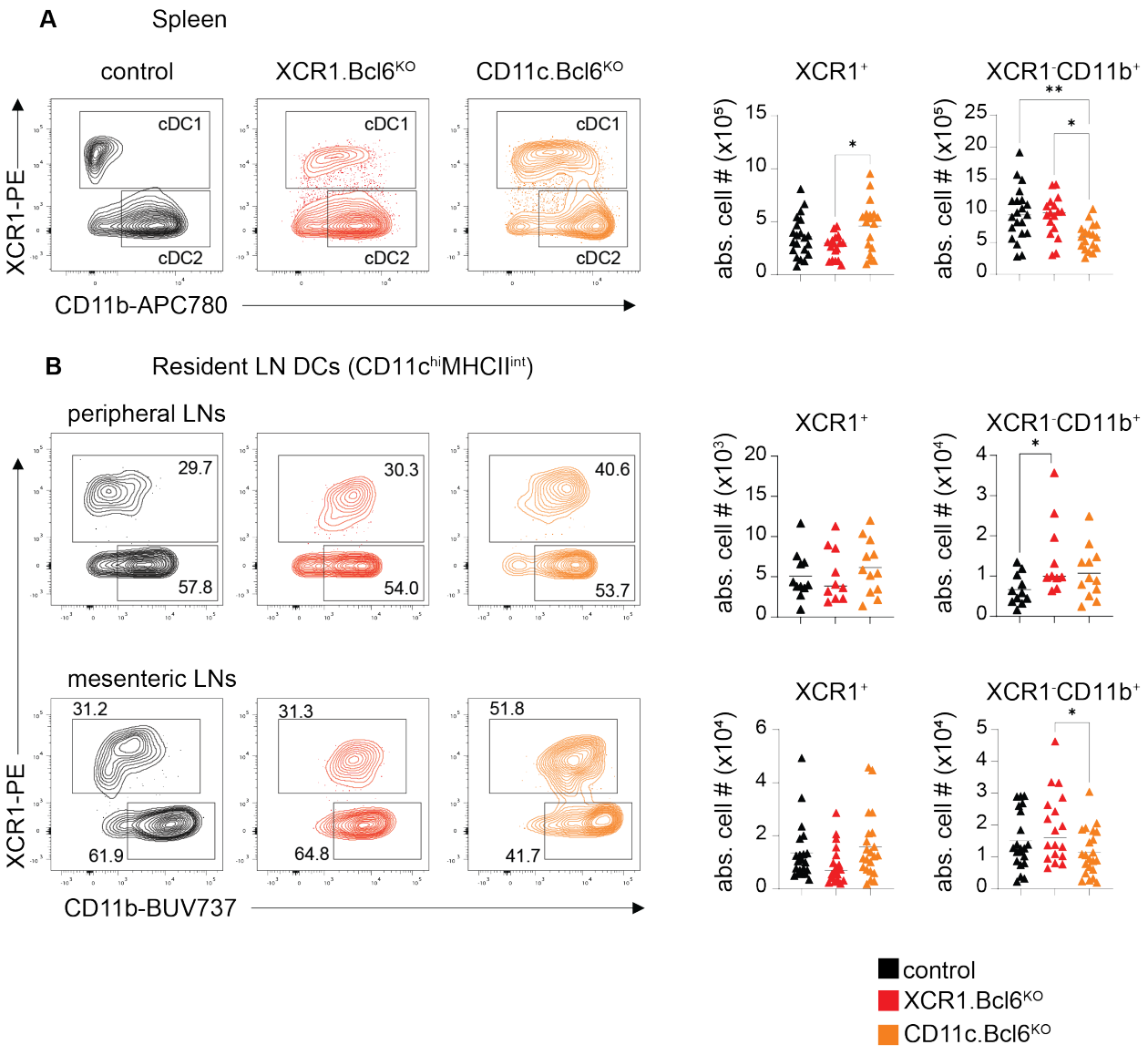

981

982

983

984

985

986

987

988 **Figure 2**

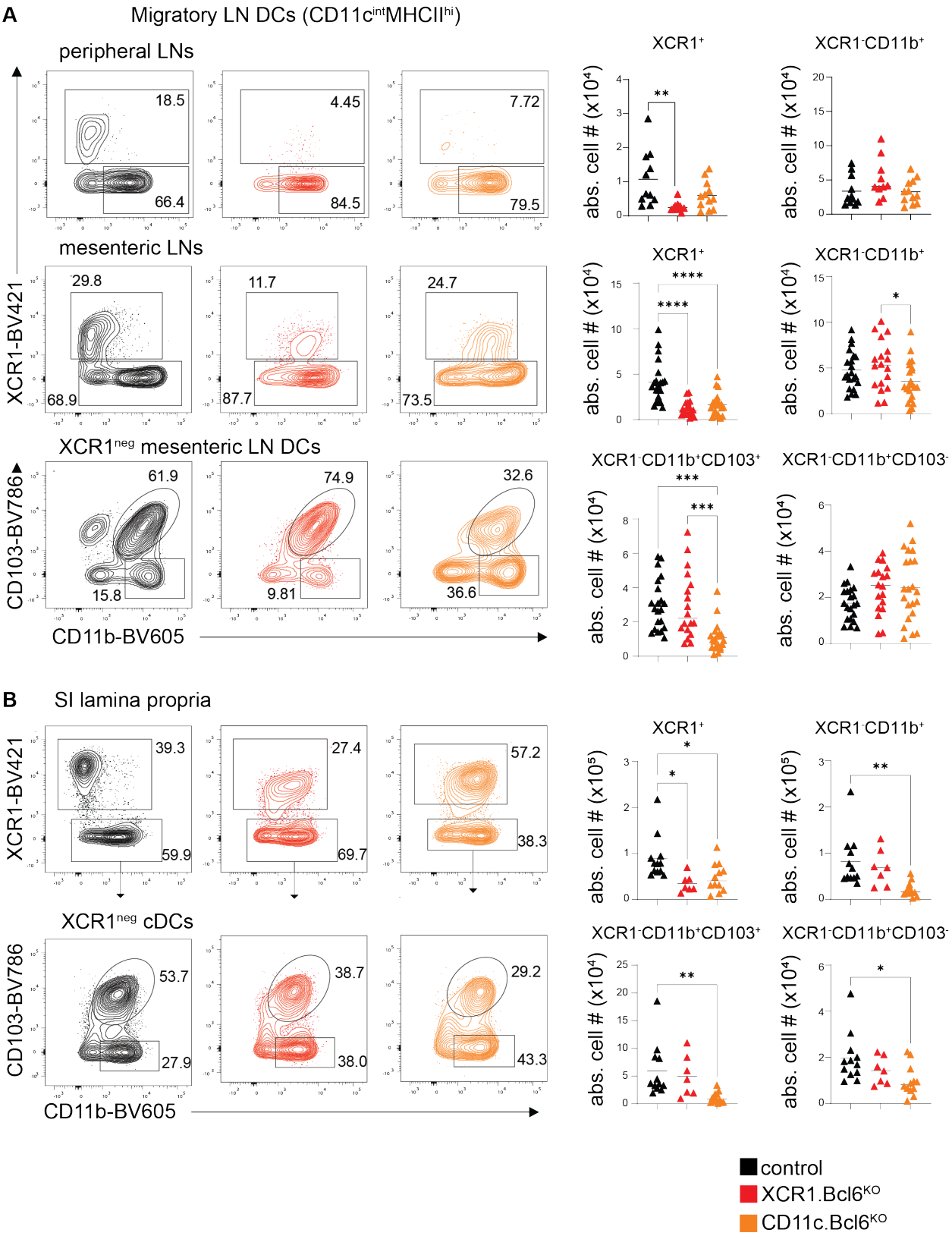

989

990 **Figure 3**

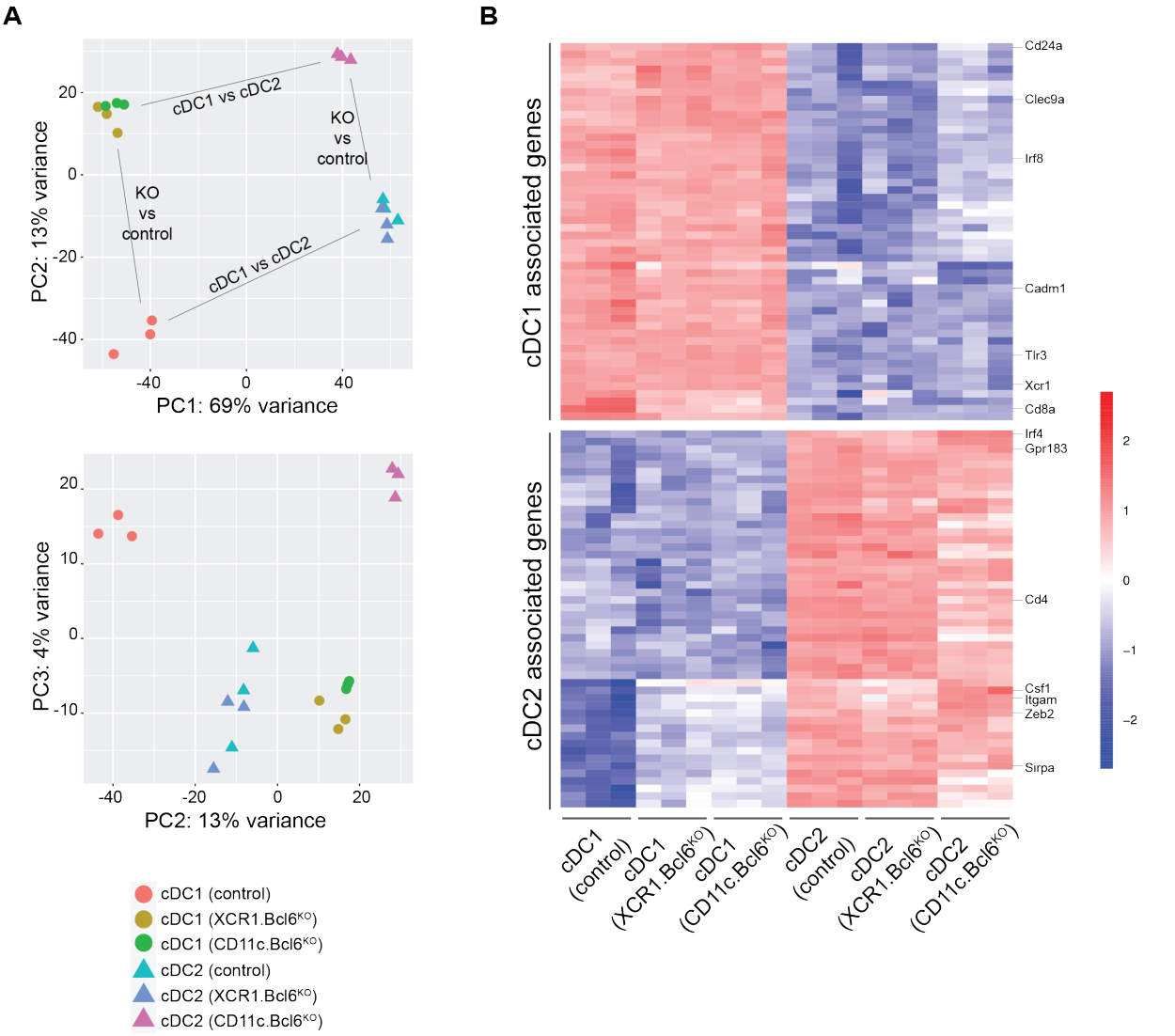

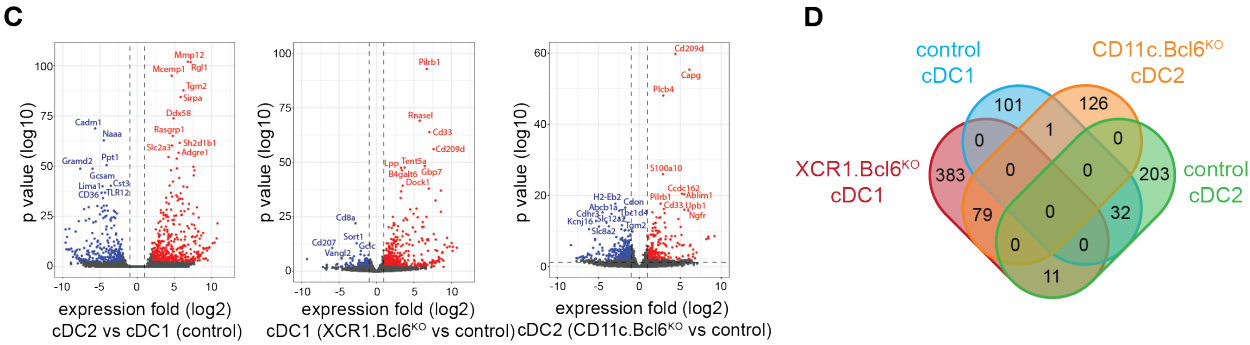

991

992

993

994 **Figure 4**

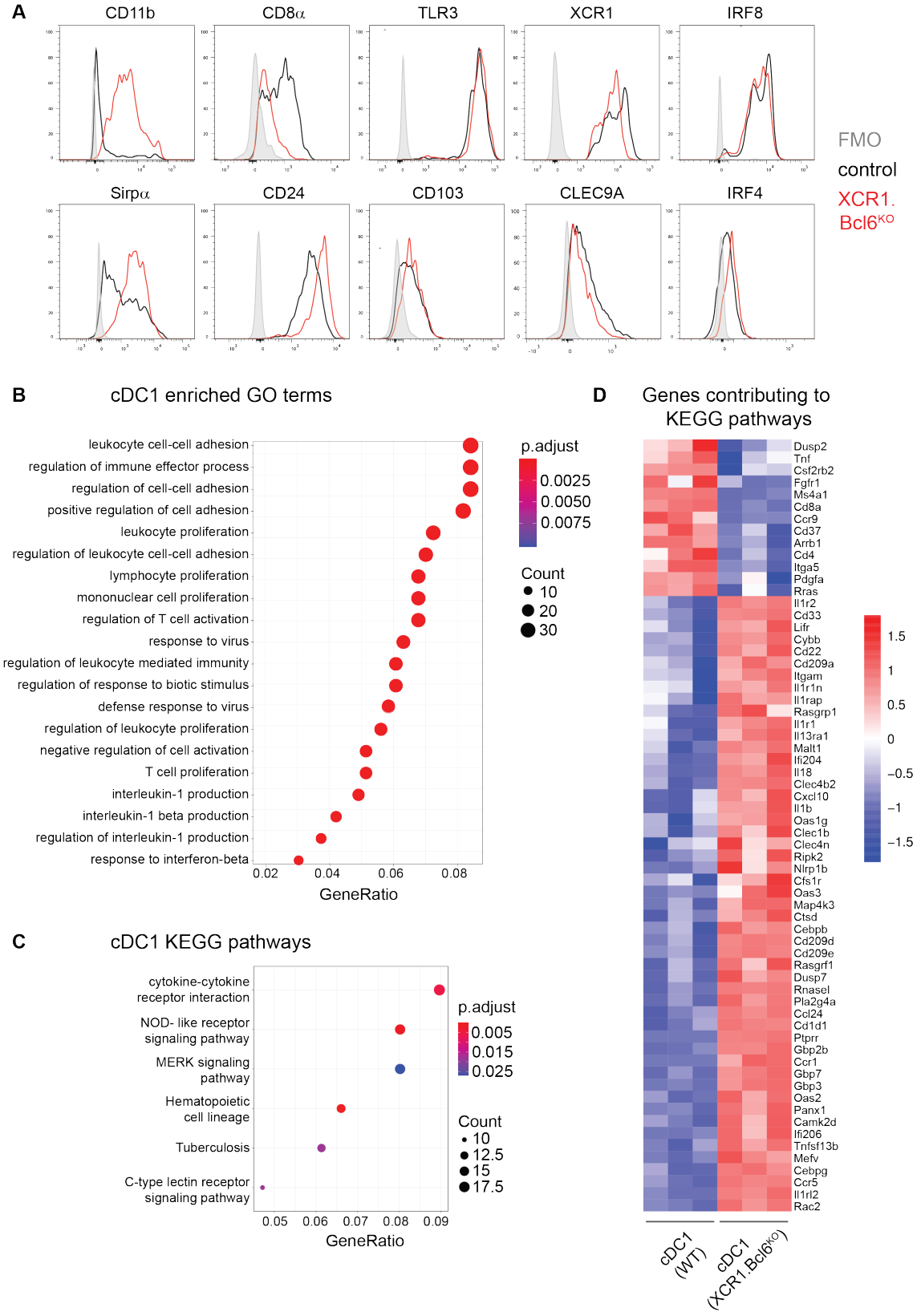

995

996 **Figure 5**

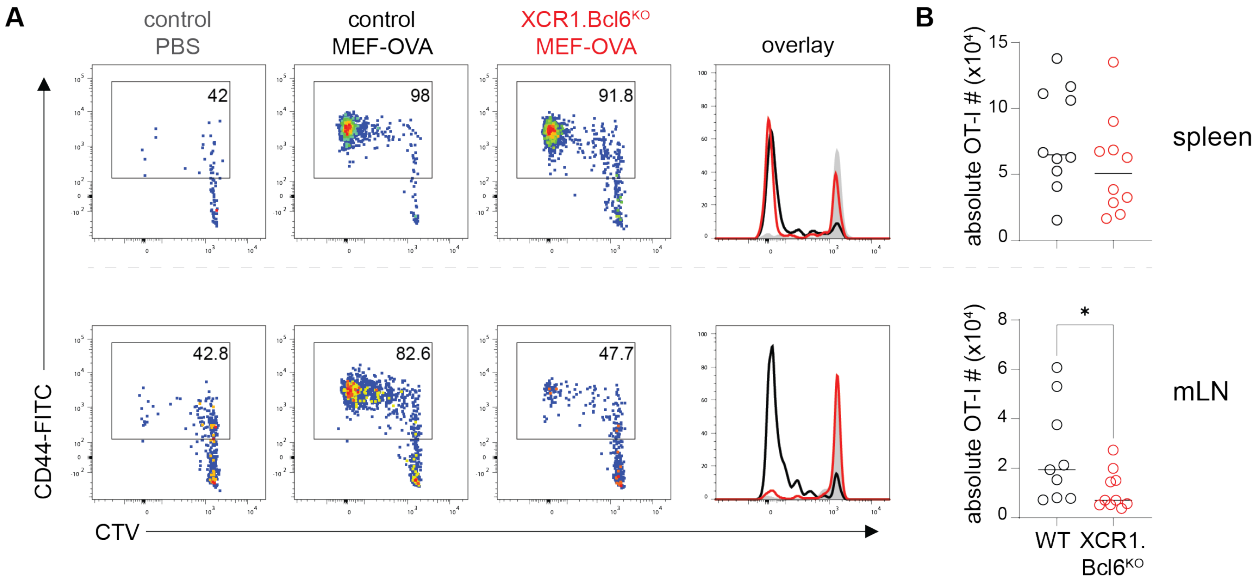

997

998

999

1000

1001

1002

1003

1004

1005

1006

1007

1008

1009

1010

1011

1012 **Figure 6**

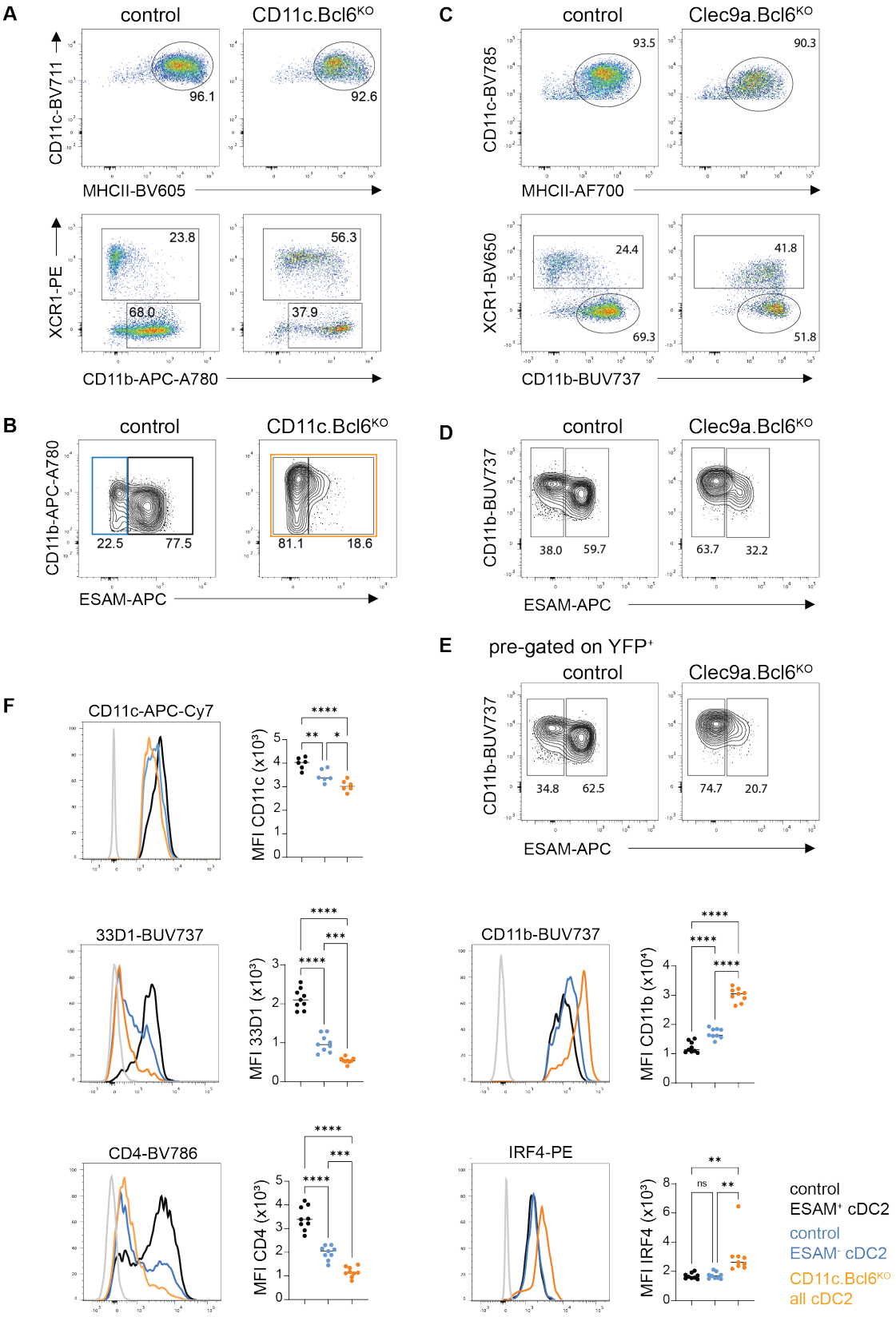

1013

1014 **Figure 7**

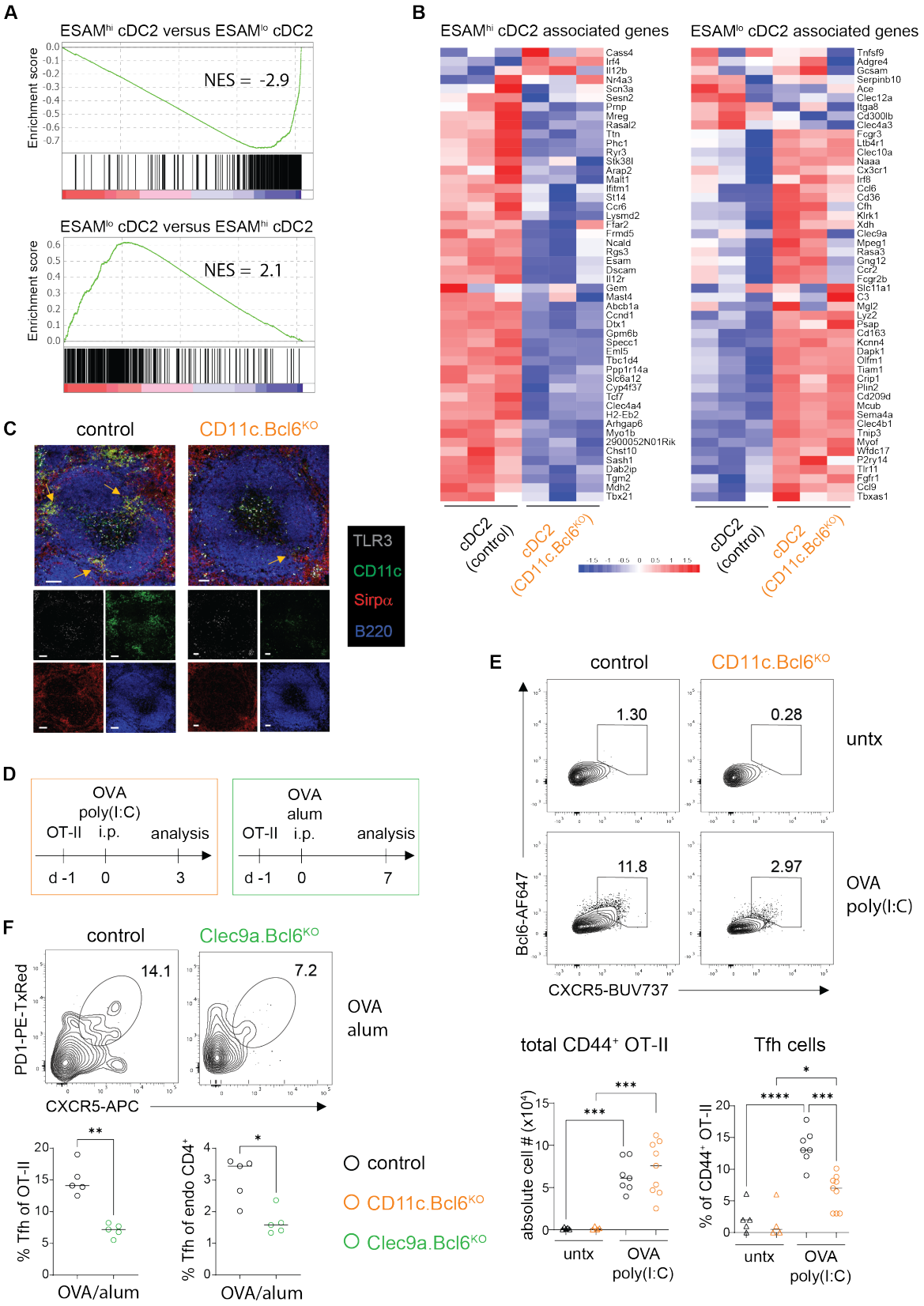

1015

1016 **Figure 8**

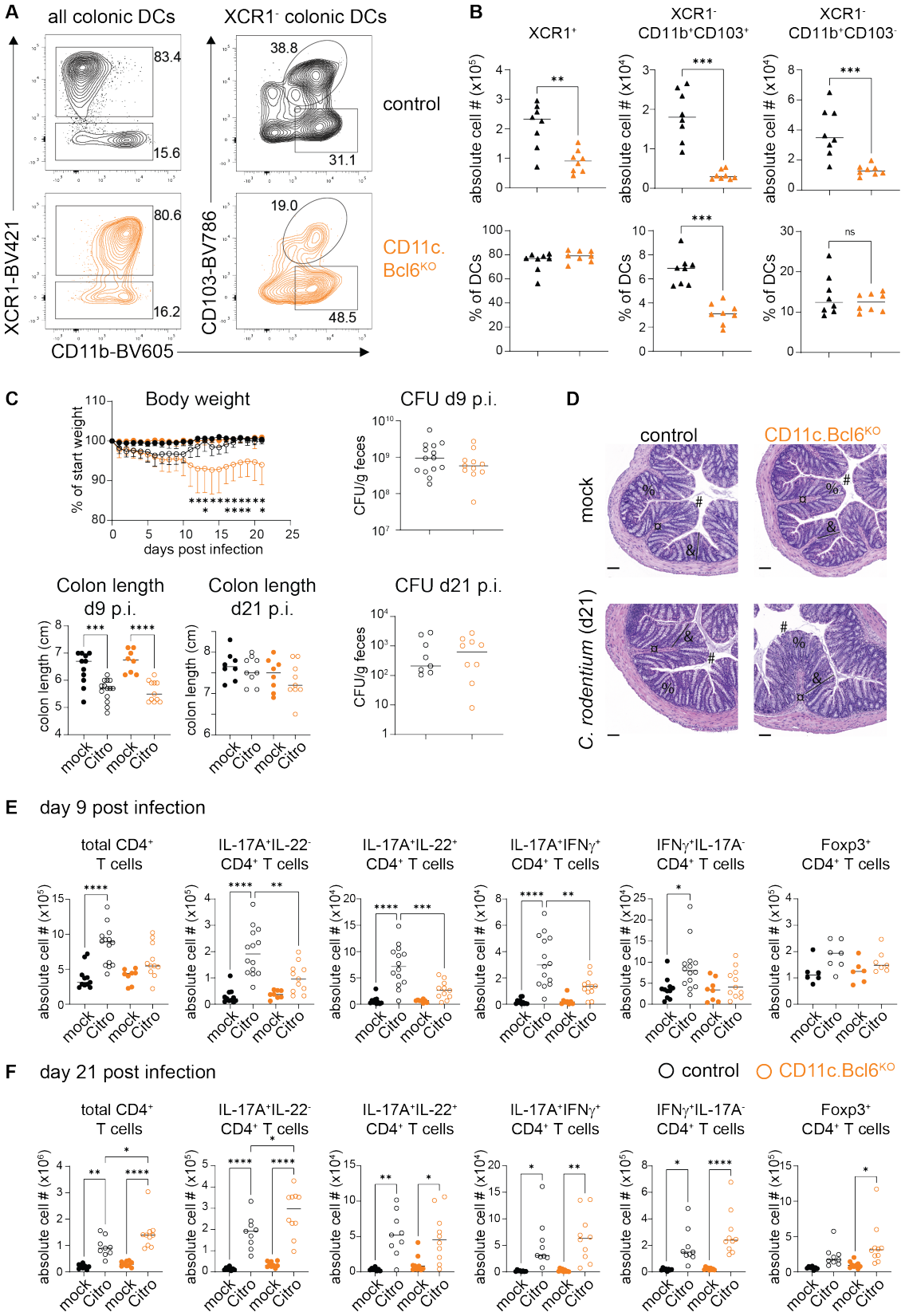

1017

1018

Supplementary Figure 1

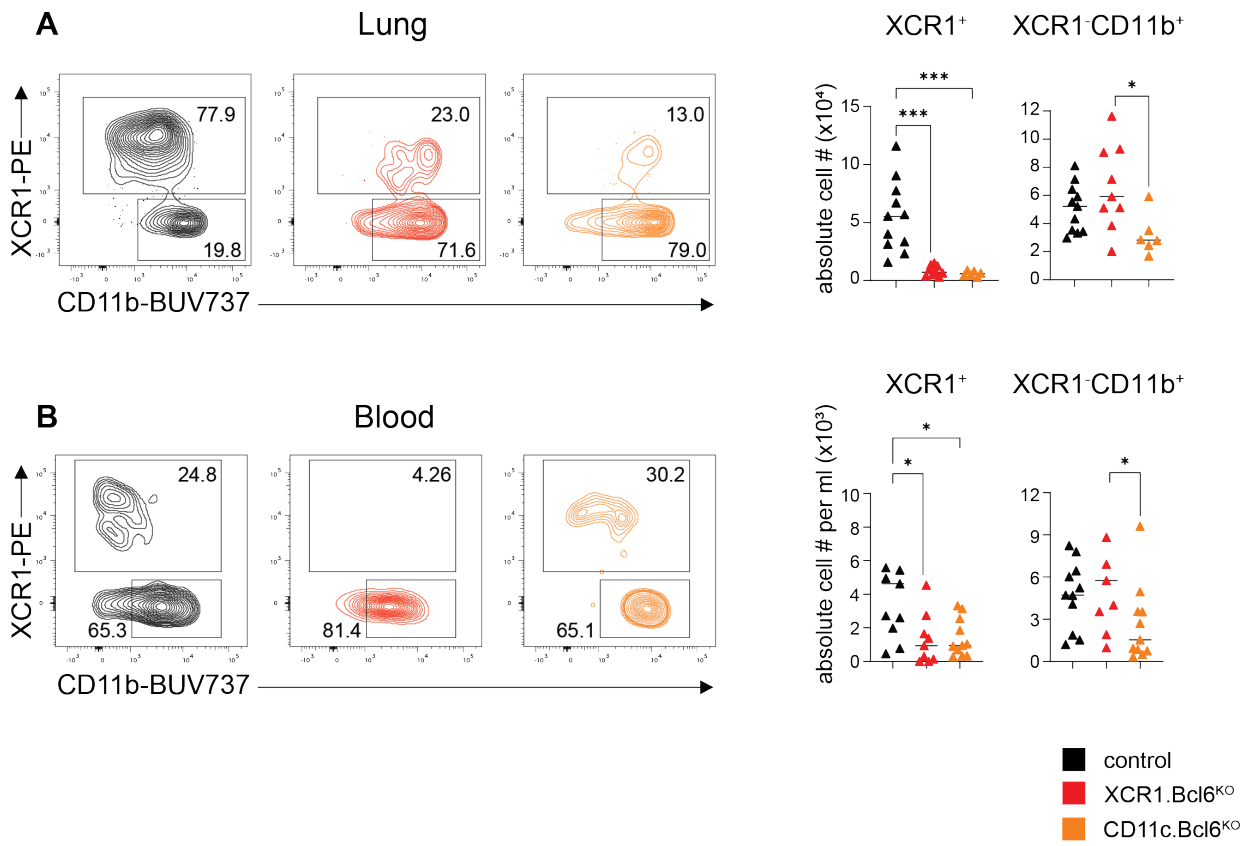

1019

1020

1021

1022

Supplementary Figure 2

A Relative abundance of cDC subsets in the spleen in Clec9a.Bcl6^{KO} and CD11c.Bcl6^{KO} mice

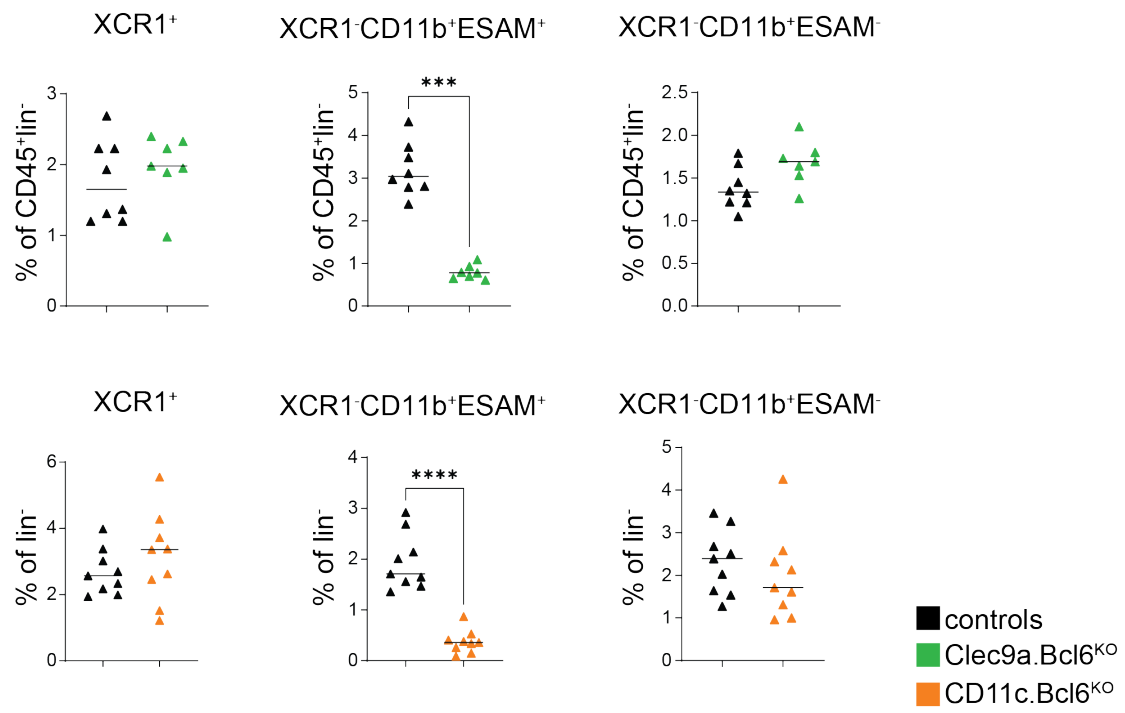

B Absolute count of cDC subsets in the spleen in Clec9a.Bcl6^{KO} and CD11c.Bcl6^{KO} mice

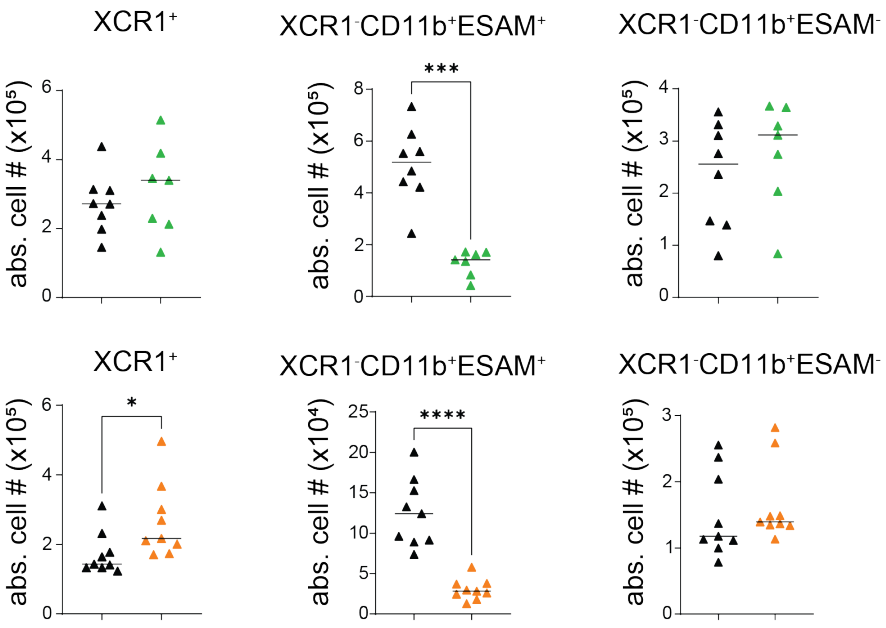

1023

Supplementary Figure 3

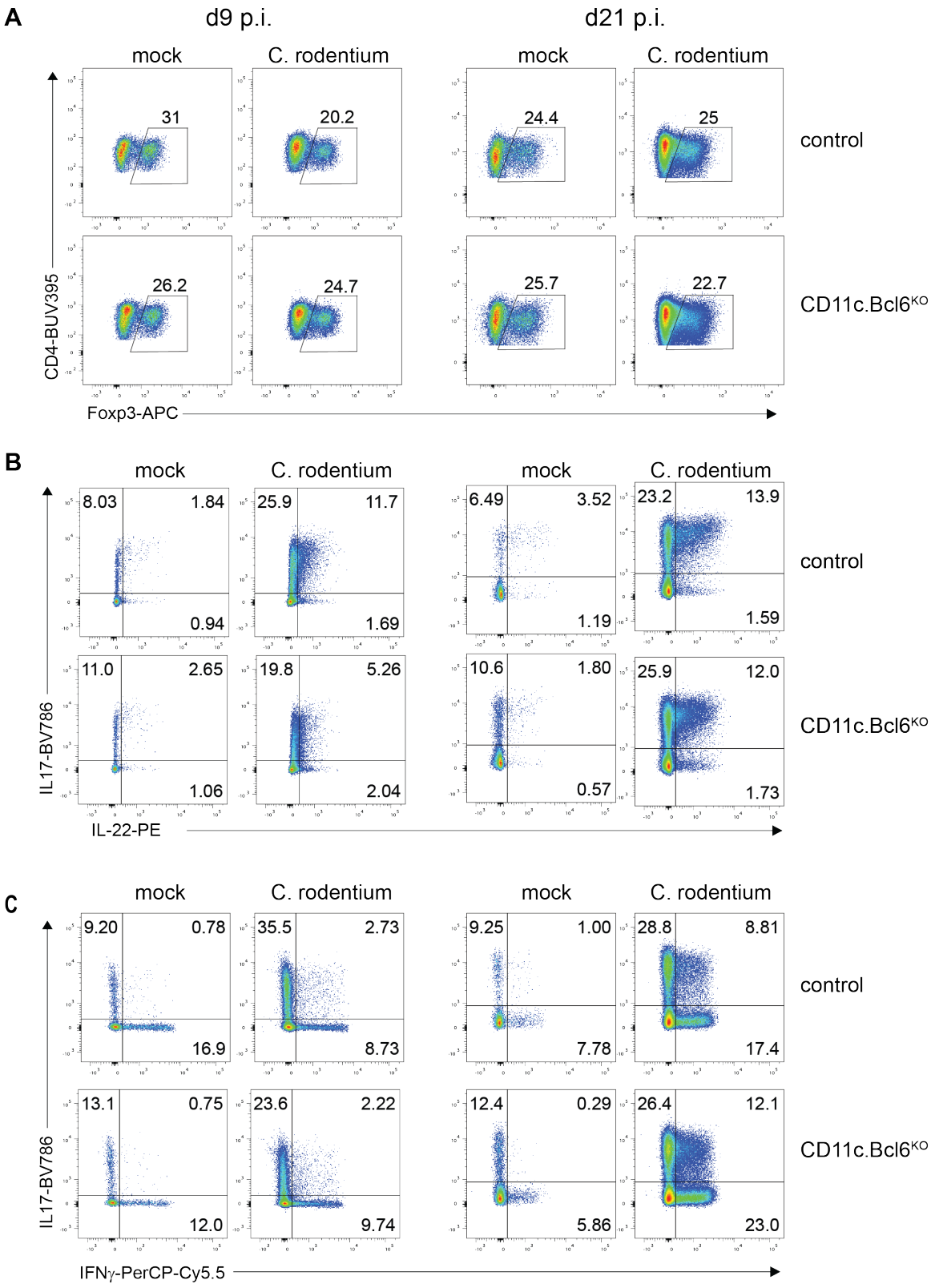

1024